

Observation and study of baryonic B decays:
 $B \rightarrow D^{(*)}p\bar{p}$, $D^{(*)}p\bar{p}\pi$, and $D^{(*)}p\bar{p}\pi\pi$

The *BABAR* Collaboration

November 4, 2018

ABSTRACT

We present a study of ten B -meson decays to a $D^{(*)}$, a proton-antiproton pair, and a system of up to two pions using *BABAR*'s data set of 455×10^6 $B\bar{B}$ pairs. Four of the modes ($\bar{B}^0 \rightarrow D^0p\bar{p}$, $\bar{B}^0 \rightarrow D^{*0}p\bar{p}$, $\bar{B}^0 \rightarrow D^+p\bar{p}\pi^-$, $\bar{B}^0 \rightarrow D^{ast+}p\bar{p}\pi^-$) are studied with improved statistics compared to previous measurements; six of the modes ($B^- \rightarrow D^0p\bar{p}\pi^-$, $B^- \rightarrow D^{*0}p\bar{p}\pi^-$, $\bar{B}^0 \rightarrow D^0p\bar{p}\pi^-\pi^+$, $\bar{B}^0 \rightarrow D^{*0}p\bar{p}\pi^-\pi^+$, $B^- \rightarrow D^+p\bar{p}\pi^-\pi^-$, $B^- \rightarrow D^{ast+}p\bar{p}\pi^-\pi^-$) are first observations. The branching fractions for 3- and 5-body decays are suppressed compared to 4-body decays. Kinematic distributions for 3-body decays show non-overlapping threshold enhancements in $m(p\bar{p})$ and $m(D^{(*)0}p)$ in the Dalitz plots. For 4-body decays, $m(p\pi^-)$ mass projections show a narrow peak with mass and full width of $(1497.4 \pm 3.0 \pm 0.9)$ MeV/ c^2 and $(47 \pm 12 \pm 4)$ MeV/ c^2 , respectively, where the first (second) errors are statistical (systematic). For 5-body decays, mass projections are similar to phase space expectations. All results are preliminary.

Submitted to the XXIV International Symposium on Lepton Photon
Interactions at High Energies,
August 17–22, 2009, Hamburg, Germany.

The BABAR Collaboration,

B. Aubert, Y. Karyotakis, J. P. Lees, V. Poireau, E. Prencipe, X. Prudent, V. Tisserand
*Laboratoire d'Annecy-le-Vieux de Physique des Particules (LAPP), Université de Savoie, CNRS/IN2P3,
F-74941 Annecy-Le-Vieux, France*

J. Garra Tico, E. Grauges
Universitat de Barcelona, Facultat de Física, Departament ECM, E-08028 Barcelona, Spain

M. Martinelli^{ab}, A. Palano^{ab}, M. Pappagallo^{ab}
INFN Sezione di Bari^a; Dipartimento di Fisica, Università di Bari^b, I-70126 Bari, Italy

G. Eigen, B. Stugu, L. Sun
University of Bergen, Institute of Physics, N-5007 Bergen, Norway

M. Battaglia, D. N. Brown, B. Hooberman, L. T. Kerth, Yu. G. Kolomensky, G. Lynch, I. L. Osipenkov,
K. Tackmann, T. Tanabe
Lawrence Berkeley National Laboratory and University of California, Berkeley, California 94720, USA

C. M. Hawkes, N. Soni, A. T. Watson
University of Birmingham, Birmingham, B15 2TT, United Kingdom

H. Koch, T. Schroeder
Ruhr Universität Bochum, Institut für Experimentalphysik 1, D-44780 Bochum, Germany

D. J. Asgeirsson, C. Hearty, T. S. Mattison, J. A. McKenna
University of British Columbia, Vancouver, British Columbia, Canada V6T 1Z1

M. Barrett, A. Khan, A. Randle-Conde
Brunel University, Uxbridge, Middlesex UB8 3PH, United Kingdom

V. E. Blinov, A. D. Bukin,^a A. R. Buzykaev, V. P. Druzhinin, V. B. Golubev, A. P. Onuchin,
S. I. Serednyakov, Yu. I. Skovpen, E. P. Solodov, K. Yu. Todyshev
Budker Institute of Nuclear Physics, Novosibirsk 630090, Russia

M. Bondioli, S. Curry, I. Eschrich, D. Kirkby, A. J. Lankford, P. Lund, M. Mandelkern, E. C. Martin,
D. P. Stoker
University of California at Irvine, Irvine, California 92697, USA

H. Atmacan, J. W. Gary, F. Liu, O. Long, G. M. Vitug, Z. Yasin
University of California at Riverside, Riverside, California 92521, USA

V. Sharma
University of California at San Diego, La Jolla, California 92093, USA

C. Campagnari, T. M. Hong, D. Kovalskyi, M. A. Mazur, J. D. Richman
University of California at Santa Barbara, Santa Barbara, California 93106, USA

T. W. Beck, A. M. Eisner, C. A. Heusch, J. Kroseberg, W. S. Lockman, A. J. Martinez, T. Schalk,
B. A. Schumm, A. Seiden, L. Wang, L. O. Winstrom
University of California at Santa Cruz, Institute for Particle Physics, Santa Cruz, California 95064, USA

^a Deceased

C. H. Cheng, D. A. Doll, B. Echenard, F. Fang, D. G. Hitlin, I. Narsky, P. Ongmongkolkul, T. Piatenko,
F. C. Porter

California Institute of Technology, Pasadena, California 91125, USA

R. Andreassen, G. Mancinelli, B. T. Meadows, K. Mishra, M. D. Sokoloff

University of Cincinnati, Cincinnati, Ohio 45221, USA

P. C. Bloom, W. T. Ford, A. Gaz, J. F. Hirschauer, M. Nagel, U. Nauenberg, J. G. Smith, S. R. Wagner

University of Colorado, Boulder, Colorado 80309, USA

R. Ayad,^b W. H. Toki

Colorado State University, Fort Collins, Colorado 80523, USA

E. Feltresi, A. Hauke, H. Jasper, T. M. Karbach, J. Merkel, A. Petzold, B. Spaan, K. Wacker

Technische Universität Dortmund, Fakultät Physik, D-44221 Dortmund, Germany

M. J. Kobel, R. Nogowski, K. R. Schubert, R. Schwierz

Technische Universität Dresden, Institut für Kern- und Teilchenphysik, D-01062 Dresden, Germany ,

D. Bernard, E. Latour, M. Verderi

Laboratoire Leprince-Ringuet, CNRS/IN2P3, Ecole Polytechnique, F-91128 Palaiseau, France

P. J. Clark, S. Playfer, J. E. Watson

University of Edinburgh, Edinburgh EH9 3JZ, United Kingdom

M. Andreotti^{ab}, D. Bettoni^a, C. Bozzi^a, R. Calabrese^{ab}, A. Cecchi^{ab}, G. Cibinetto^{ab}, E. Fioravanti^{ab}
P. Franchini^{ab}, E. Luppi^{ab}, M. Menerato^{ab}, M. Negrini^{ab}, A. Petrella^{ab}, L. Piemontese^a, V. Santoro^{ab}

INFN Sezione di Ferrara^a; Dipartimento di Fisica, Università di Ferrara^b, I-44100 Ferrara, Italy

R. Baldini-Ferroli, A. Calcaterra, R. de Sangro, G. Finocchiaro, S. Pacetti, P. Patteri, I. M. Peruzzi,^c
M. Piccolo, M. Rama, A. Zallo

INFN Laboratori Nazionali di Frascati, I-00044 Frascati, Italy

R. Contri^{ab}, E. Guido^{ab}, M. Lo Vetere^{ab}, M. R. Monge^{ab}, S. Passaggio^a, C. Patrignani^{ab}, E. Robutti^a,
S. Tosi^{ab}

INFN Sezione di Genova^a; Dipartimento di Fisica, Università di Genova^b, I-16146 Genova, Italy

M. Morii

Harvard University, Cambridge, Massachusetts 02138, USA

A. Adametz, J. Marks, S. Schenk, U. Uwer

Universität Heidelberg, Physikalisches Institut, Philosophenweg 12, D-69120 Heidelberg, Germany

F. U. Bernlochner, H. M. Lacker, T. Lueck, A. Volk

Humboldt-Universität zu Berlin, Institut für Physik, Newtonstr. 15, D-12489 Berlin, Germany

P. D. Dauncey, M. Tibbetts

Imperial College London, London, SW7 2AZ, United Kingdom

^b Now at Temple University, Philadelphia, Pennsylvania 19122, USA

^c Also with Università di Perugia, Dipartimento di Fisica, Perugia, Italy

P. K. Behera, M. J. Charles, U. Mallik

University of Iowa, Iowa City, Iowa 52242, USA

J. Cochran, H. B. Crawley, L. Dong, V. Eyges, W. T. Meyer, S. Prell, E. I. Rosenberg, A. E. Rubin

Iowa State University, Ames, Iowa 50011-3160, USA

Y. Y. Gao, A. V. Gritsan, Z. J. Guo

Johns Hopkins University, Baltimore, Maryland 21218, USA

N. Arnaud, A. D’Orazio, M. Davier, D. Derkach, J. Firmino da Costa, G. Grosdidier, F. Le Diberder,
V. Lepeltier, A. M. Lutz, B. Malaescu, P. Roudeau, M. H. Schune, J. Serrano, V. Sordini,^d A. Stocchi,
G. Wormser

*Laboratoire de l’Accélérateur Linéaire, IN2P3/CNRS et Université Paris-Sud 11, Centre Scientifique
d’Orsay, B. P. 34, F-91898 Orsay Cedex, France*

D. J. Lange, D. M. Wright

Lawrence Livermore National Laboratory, Livermore, California 94550, USA

I. Bingham, J. P. Burke, C. A. Chavez, J. R. Fry, E. Gabathuler, R. Gamet, D. E. Hutchcroft, D. J. Payne,
C. Touramanis

University of Liverpool, Liverpool L69 7ZE, United Kingdom

A. J. Bevan, C. K. Clarke, F. Di Lodovico, R. Sacco, M. Sigamani

Queen Mary, University of London, London, E1 4NS, United Kingdom

G. Cowan, S. Paramesvaran, A. C. Wren

*University of London, Royal Holloway and Bedford New College, Egham, Surrey TW20 0EX, United
Kingdom*

D. N. Brown, C. L. Davis

University of Louisville, Louisville, Kentucky 40292, USA

A. G. Denig, M. Fritsch, W. Gradl, A. Hafner

Johannes Gutenberg-Universität Mainz, Institut für Kernphysik, D-55099 Mainz, Germany

K. E. Alwyn, D. Bailey, R. J. Barlow, G. Jackson, G. D. Lafferty, T. J. West, J. I. Yi

University of Manchester, Manchester M13 9PL, United Kingdom

J. Anderson, C. Chen, A. Jawahery, D. A. Roberts, G. Simi, J. M. Tuggle

University of Maryland, College Park, Maryland 20742, USA

C. Dallapiccola, E. Salvati

University of Massachusetts, Amherst, Massachusetts 01003, USA

R. Cowan, D. Dujmic, P. H. Fisher, S. W. Henderson, G. Sciolla, M. Spitznagel, R. K. Yamamoto, M. Zhao
*Massachusetts Institute of Technology, Laboratory for Nuclear Science, Cambridge, Massachusetts 02139,
USA*

P. M. Patel, S. H. Robertson, M. Schram

McGill University, Montréal, Québec, Canada H3A 2T8

^d Also with Università di Roma La Sapienza, I-00185 Roma, Italy

P. Biassoni^{ab}, A. Lazzaro^{ab}, V. Lombardo^a, F. Palombo^{ab}, S. Stracka^{ab}
INFN Sezione di Milano^a; Dipartimento di Fisica, Università di Milano^b, I-20133 Milano, Italy

L. Cremaldi, R. Godang,^e R. Kroeger, P. Sonnek, D. J. Summers, H. W. Zhao
University of Mississippi, University, Mississippi 38677, USA

X. Nguyen, M. Simard, P. Taras
Université de Montréal, Physique des Particules, Montréal, Québec, Canada H3C 3J7

H. Nicholson
Mount Holyoke College, South Hadley, Massachusetts 01075, USA

G. De Nardo^{ab}, L. Lista^a, D. Monorchio^{ab}, G. Onorato^{ab}, C. Sciacca^{ab}
INFN Sezione di Napoli^a; Dipartimento di Scienze Fisiche, Università di Napoli Federico II^b, I-80126 Napoli, Italy

G. Raven, H. L. Snoek
NIKHEF, National Institute for Nuclear Physics and High Energy Physics, NL-1009 DB Amsterdam, The Netherlands

C. P. Jessop, K. J. Knoepfel, J. M. LoSecco, W. F. Wang
University of Notre Dame, Notre Dame, Indiana 46556, USA

L. A. Corwin, K. Honscheid, H. Kagan, R. Kass, J. P. Morris, A. M. Rahimi, S. J. Sekula
Ohio State University, Columbus, Ohio 43210, USA

N. L. Blount, J. Brau, R. Frey, O. Igonkina, J. A. Kolb, M. Lu, R. Rahmat, N. B. Sinev, D. Strom,
J. Strube, E. Torrence
University of Oregon, Eugene, Oregon 97403, USA

G. Castelli^{ab}, N. Gagliardi^{ab}, M. Margoni^{ab}, M. Morandin^a, M. Posocco^a, M. Rotondo^a, F. Simonetto^{ab},
R. Stroili^{ab}, C. Voci^{ab}
INFN Sezione di Padova^a; Dipartimento di Fisica, Università di Padova^b, I-35131 Padova, Italy

P. del Amo Sanchez, E. Ben-Haim, G. R. Bonneaud, H. Briand, J. Chauveau, O. Hamon, Ph. Leruste,
G. Marchiori, J. Ocariz, A. Perez, J. Prendki, S. Sitt
Laboratoire de Physique Nucléaire et de Hautes Energies, IN2P3/CNRS, Université Pierre et Marie Curie-Paris6, Université Denis Diderot-Paris7, F-75252 Paris, France

L. Gladney
University of Pennsylvania, Philadelphia, Pennsylvania 19104, USA

M. Biasini^{ab}, E. Manoni^{ab}
INFN Sezione di Perugia^a; Dipartimento di Fisica, Università di Perugia^b, I-06100 Perugia, Italy

C. Angelini^{ab}, G. Batignani^{ab}, S. Bettarini^{ab}, G. Calderini^{ab,f}, M. Carpinelli^{ab,g}, A. Cervelli^{ab}, F. Forti^{ab},
M. A. Giorgi^{ab}, A. Lusiani^{ac}, M. Morganti^{ab}, N. Neri^{ab}, E. Paoloni^{ab}, G. Rizzo^{ab}, J. J. Walsh^a
INFN Sezione di Pisa^a; Dipartimento di Fisica, Università di Pisa^b; Scuola Normale Superiore di Pisa^c, I-56127 Pisa, Italy

^e Now at University of South Alabama, Mobile, Alabama 36688, USA

^f Also with Laboratoire de Physique Nucléaire et de Hautes Energies, IN2P3/CNRS, Université Pierre et Marie Curie-Paris6, Université Denis Diderot-Paris7, F-75252 Paris, France

^g Also with Università di Sassari, Sassari, Italy

D. Lopes Pegna, C. Lu, J. Olsen, A. J. S. Smith, A. V. Telnov
Princeton University, Princeton, New Jersey 08544, USA

F. Anulli^a, E. Baracchini^{ab}, G. Cavoto^a, R. Faccini^{ab}, F. Ferrarotto^a, F. Ferroni^{ab}, M. Gaspero^{ab},
P. D. Jackson^a, L. Li Gioi^a, M. A. Mazzoni^a, S. Morganti^a, G. Piredda^a, F. Renga^{ab}, C. Voena^a
INFN Sezione di Roma^a; Dipartimento di Fisica, Università di Roma La Sapienza^b, I-00185 Roma, Italy

M. Ebert, T. Hartmann, H. Schröder, R. Waldi
Universität Rostock, D-18051 Rostock, Germany

T. Adye, B. Franek, E. O. Olaiya, F. F. Wilson
Rutherford Appleton Laboratory, Chilton, Didcot, Oxon, OX11 0QX, United Kingdom

S. Emery, L. Esteve, G. Hamel de Monchenault, W. Kozanecki, G. Vasseur, Ch. Yèche, M. Zito
CEA, Irfu, SPP, Centre de Saclay, F-91191 Gif-sur-Yvette, France

M. T. Allen, D. Aston, D. J. Bard, R. Bartoldus, J. F. Benitez, R. Cenci, J. P. Coleman, M. R. Convery,
J. C. Dingfelder, J. Dorfan, G. P. Dubois-Felsmann, W. Dunwoodie, R. C. Field, M. Franco Sevilla,
B. G. Fulsom, A. M. Gabareen, M. T. Graham, P. Grenier, C. Hast, W. R. Innes, J. Kaminski,
M. H. Kelsey, H. Kim, P. Kim, M. L. Kocian, D. W. G. S. Leith, S. Li, B. Lindquist, S. Luitz, V. Luth,
H. L. Lynch, D. B. MacFarlane, H. Marsiske, R. Messner,^h D. R. Muller, H. Neal, S. Nelson,
C. P. O'Grady, I. Ofte, M. Perl, B. N. Ratcliff, A. Roodman, A. A. Salnikov, R. H. Schindler,
J. Schwiening, A. Snyder, D. Su, M. K. Sullivan, K. Suzuki, S. K. Swain, J. M. Thompson, J. Va'vra,
A. P. Wagner, M. Weaver, C. A. West, W. J. Wisniewski, M. Wittgen, D. H. Wright, H. W. Wulsin,
A. K. Yarritu, C. C. Young, V. Ziegler

SLAC National Accelerator Laboratory, Stanford, California 94309 USA

X. R. Chen, H. Liu, W. Park, M. V. Purohit, R. M. White, J. R. Wilson
University of South Carolina, Columbia, South Carolina 29208, USA

M. Bellis, P. R. Burchat, A. J. Edwards, T. S. Miyashita
Stanford University, Stanford, California 94305-4060, USA

S. Ahmed, M. S. Alam, J. A. Ernst, B. Pan, M. A. Saeed, S. B. Zain
State University of New York, Albany, New York 12222, USA

A. Soffer

Tel Aviv University, School of Physics and Astronomy, Tel Aviv, 69978, Israel

S. M. Spanier, B. J. Wogslund
University of Tennessee, Knoxville, Tennessee 37996, USA

R. Eckmann, J. L. Ritchie, A. M. Ruland, C. J. Schilling, R. F. Schwitters, B. C. Wray
University of Texas at Austin, Austin, Texas 78712, USA

B. W. Drummond, J. M. Izen, X. C. Lou
University of Texas at Dallas, Richardson, Texas 75083, USA

F. Bianchi^{ab}, D. Gamba^{ab}, M. Pelliccioni^{ab}
INFN Sezione di Torino^a; Dipartimento di Fisica Sperimentale, Università di Torino^b, I-10125 Torino, Italy

^h Deceased

M. Bomben^{ab}, L. Bosisio^{ab}, C. Cartaro^{ab}, G. Della Ricca^{ab}, L. Lanceri^{ab}, L. Vitale^{ab}
INFN Sezione di Trieste^a; Dipartimento di Fisica, Università di Trieste^b, I-34127 Trieste, Italy

V. Azzolini, N. Lopez-March, F. Martinez-Vidal, D. A. Milanes, A. Oyanguren
IFIC, Universitat de Valencia-CSIC, E-46071 Valencia, Spain

J. Albert, Sw. Banerjee, B. Bhuyan, H. H. F. Choi, K. Hamano, G. J. King, R. Kowalewski,
M. J. Lewczuk, I. M. Nugent, J. M. Roney, R. J. Sobie
University of Victoria, Victoria, British Columbia, Canada V8W 3P6

T. J. Gershon, P. F. Harrison, J. Ilic, T. E. Latham, G. B. Mohanty, E. M. T. Puccio
Department of Physics, University of Warwick, Coventry CV4 7AL, United Kingdom

H. R. Band, X. Chen, S. Dasu, K. T. Flood, Y. Pan, R. Prepost, C. O. Vuosalo, S. L. Wu
University of Wisconsin, Madison, Wisconsin 53706, USA

I. INTRODUCTION

The decaysⁱ of B mesons to final states with baryons have been explored much less systematically than decays to meson-only final states. Such decays have their own distinctive features; in particular, the suppression of the rate for two-body decays and the rate enhancement for low masses of the baryon-antibaryon system in multi-body decays [1, 2, 3, 4, 5, 6, 7]. The first observed exclusive decays were the CLEO measurements of $B \rightarrow \Lambda_c^+ \bar{p} \pi(\pi)$ [8] followed by $\bar{B}^0 \rightarrow D^{*+} p \bar{p} \pi^-$ and $B^0 \rightarrow D^{*-} p \bar{n}$ ^j [9] supporting a prediction [10] that the decays with Λ_c are not the only significant contributions to the baryonic B decay rate and that $D^{(*)} N \bar{N}' + \text{anything}$ is also important, where N and N' are nucleons. Belle observed $\bar{B}^0 \rightarrow D^{(*)0} p \bar{p}$ [11] obtaining a branching fraction about five times smaller than for $D^{*+} p \bar{p} \pi^-$.

We report the branching fractions and kinematic distributions for ten baryonic B decays:

$$\begin{aligned}
 & \text{3-body decays } \bar{B}^0 \rightarrow D^0 p \bar{p} && \text{and } D^{*0} p \bar{p}, \\
 & \text{4-body decays } \bar{B}^0 \rightarrow D^+ p \bar{p} \pi^- && \text{and } D^{*+} p \bar{p} \pi^-, \\
 & \quad \quad \quad " \quad B^- \rightarrow D^0 p \bar{p} \pi^- && \text{and } D^{*0} p \bar{p} \pi^-, \\
 & \text{5-body decays } \bar{B}^0 \rightarrow D^0 p \bar{p} \pi^- \pi^+ && \text{and } D^{*0} p \bar{p} \pi^- \pi^+, \\
 & \quad \quad \quad " \quad B^- \rightarrow D^+ p \bar{p} \pi^- \pi^- && \text{and } D^{*+} p \bar{p} \pi^- \pi^-,
 \end{aligned} \tag{1}$$

where the latter six in the list are first observations.^k The D^* are reconstructed as $D^0 \pi^+$ and $D^0 \pi^0$; D as $K^- \pi^+$, $K^- \pi^+ \pi^0$, $K^- \pi^+ \pi^- \pi^+$, and $K^- \pi^+ \pi^+$. This makes up 26 reconstructed decay chains (3 for each of eight B decays with D^0 and 1 for two with D^+). This study uses 455×10^6 $B\bar{B}$ pairs and supersedes the previous BABAR publication of $\bar{B}^0 \rightarrow D^{(*)0} p \bar{p}$ and $D^{(*)+} p \bar{p} \pi^-$ [13] using 232×10^6 $B\bar{B}$ pairs. Figure 1 shows the typical valence-quark diagrams for 3- and 4-body decays.

Until recently, interest has focused on the dynamical features of baryonic decays, on studying rare modes (both $b \rightarrow u$ and $b \rightarrow s$ transitions), and on the role these modes play in accounting for the overall production of charm in B decays. Many theoretical studies have appeared [10, 14, 15, 16, 17, 18, 19, 20, 21, 22, 23, 24, 25, 26, 27] using the decays as a playground for phenomenological models including some with $p\bar{p}$ bound states [25] and multi-quark intermediate resonances [26].

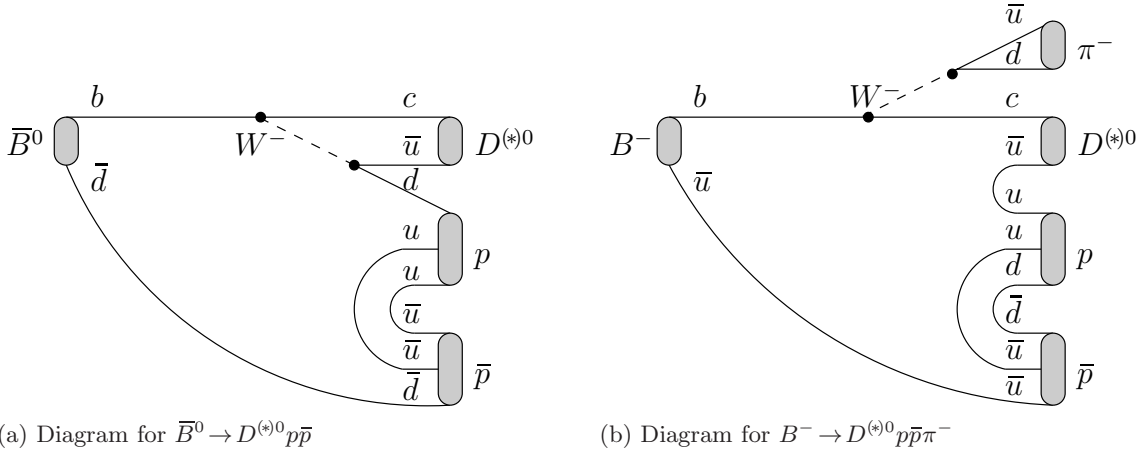


FIG. 1: Typical valence-quark diagrams for (a) 3- and (b) 4-body B decays.

ⁱ Charge conjugation of particles and decays are implied throughout this document unless otherwise stated.

^j The charge conjugate $\bar{B}^0 \rightarrow D^{*+} \bar{p} n$ is not included since CLEO only detects antineutrons \bar{n} .

^k $B^- \rightarrow D^{(*)-} p \bar{p}$ are suppressed by λ^2 [12] with respect to Fig. 1a for $b \rightarrow u D^{(*)-}$ and are beyond our sensitivity.

We hope to shed light on these models by studying the relatively unexplored territory of $b \rightarrow c$ baryonic B decays involving a $D^{(*)}$ meson.

II. THE BABAR DETECTOR AND DATA SET

The *BABAR* detector is described in detail elsewhere [28]. Exclusive B -meson decays are simulated with the Monte Carlo (MC) event generator EVTGEN [29] and hadronization is simulated with JETSET 7.4 [30]. We use GEANT4 [31] to model interactions of particles traversing the detector, taking into account the varying detector conditions and beam backgrounds.

This study uses the data set of 414 fb^{-1} collected with the *BABAR* detector at the PEP-II asymmetric-energy e^+e^- collider at the SLAC National Accelerator Laboratory. Figure 2 is a data event display of $B^0 \rightarrow \bar{D}^0 p \bar{p}$ followed by $\bar{D}^0 \rightarrow K^+ \pi^-$. For each daughter particle, we can see the drift chamber hits matching up with projected Cherenkov light cones in the ring-imaging detector.

III. ANALYSIS METHOD

A. Event selection

We select events with a B candidate reconstructed in one of 26 decay chains in Eqn. 1 in two steps:

First, the *BABAR* data set is reduced by requiring the presence of a p , \bar{p} , and D . The average momentum of a proton produced in a typical B decay listed in Eqn. 1 is $1 \text{ GeV}/c$. Protons are

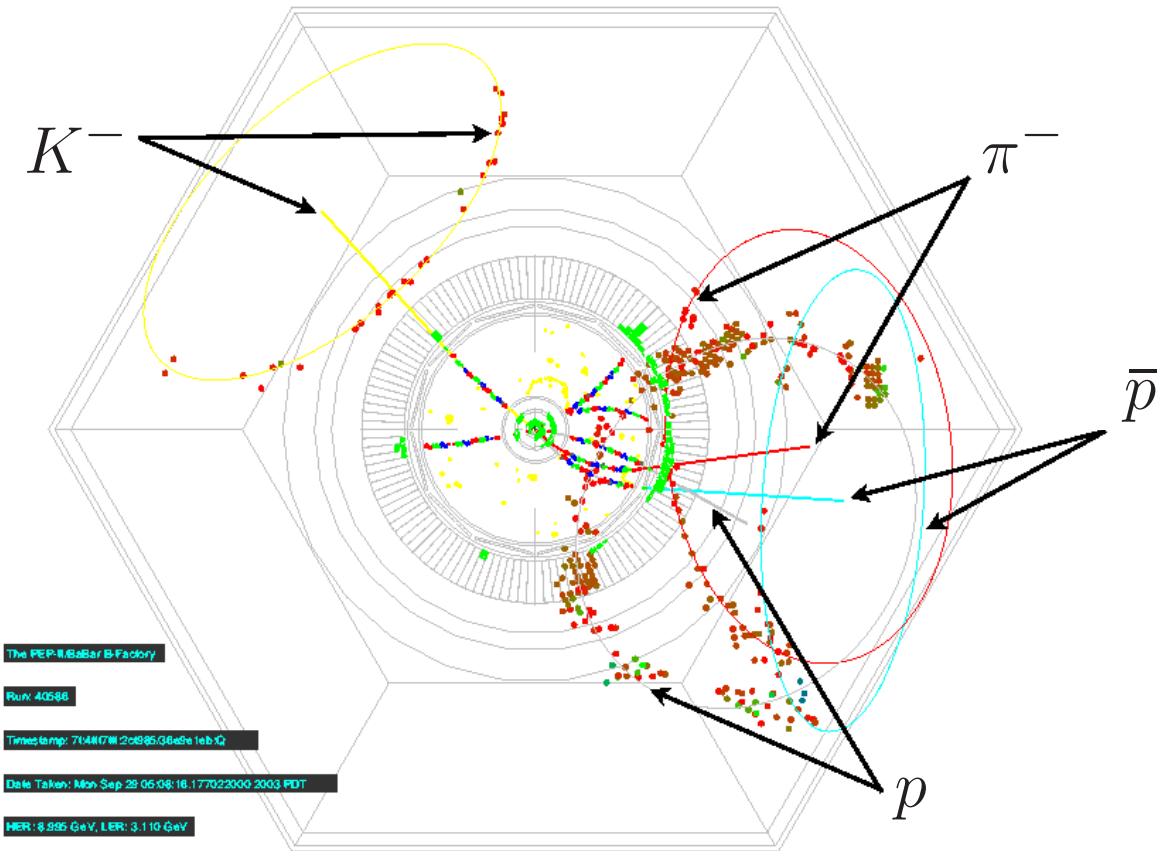


FIG. 2: Event display of $B^0 \rightarrow \bar{D}^0 p \bar{p}$, $\bar{D}^0 \rightarrow K^+ \pi^-$ transverse to the e^- beam direction.

identified with a likelihood-based selector using information from the silicon vertex tracker, drift chamber, and ring-imaging Cherenkov detector, which has a 98% selection efficiency and a 1% kaon fake rate. The D mesons decay to charged tracks and π^0 s. Charged tracks are required to be in the fiducial volume and have a distance of closest approach to the beam spot < 1.5 cm. Neutral pions are formed from two well-separated photons with $115 < m_{\gamma\gamma} < 150$ MeV/ c^2 or from two unseparated photons using the second moment of the electromagnetic calorimeter energy distribution. The same requirements apply to the non-composite daughters of B and D^* decays.

Second, the data set is further reduced by the explicit reconstruction of B candidates. B candidates are formed with a D mass [32] constraint using a Kalman fitter [33] with its vertex χ^2 probability $> 0.1\%$. To suppress continuum $e^+e^- \rightarrow q\bar{q}$ ($q = u, d, s, c$) events, we compute the angle between the thrust axes of the B candidate and the rest of the event [34]. For modes with a D^* , the mass difference $\Delta m = m(D^0\pi) - m(D^0)$ is required to be within 3σ of the nominal value, where the resolution is around 0.8 MeV/ c^2 . For $\bar{B}^0 \rightarrow D^0 p\bar{p}\pi^-\pi^+$, we require $\Delta m > 160$ MeV/ c^2 on the $D^0\pi^+$ system. For all decay modes, D candidates are required to be within 3σ around the nominal value, where the mass resolution for $K\pi$, $K\pi\pi^0$, $K\pi\pi\pi$, and $K\pi\pi$ is around 6, 10, 5, and 5 MeV/ c^2 , respectively. Furthermore, the average momentum of a kaon produced in a typical D decay is 0.9 GeV/ c and is found with the above-mentioned likelihood technique, which has an 85% selection efficiency and a 2% pion fake rate. For $K\pi\pi^0$ decays, we use the squared decay amplitude based on a Dalitz plot model [35]. Lastly, requirements are optimized by maximizing the ratio of the squared expected signal yield and its sum with expected backgrounds. For cut values with broad maxima, they are chosen to be uniform across related decay modes.

After events are filtered through the two steps, we are left with $\mathcal{O}(10^5)$ for all modes. The average number of B candidates per event that pass all requirements ranges from 1.0–1.7, increasing with the multiplicity of the decay. If there are multiple such candidates, then we choose one with the $D^{(*)}$ mass closest to the nominal value; furthermore, if candidates share a $D^{(*)}$, we choose one at random. The reconstruction efficiencies are found using MC containing the desired B decay. In general, efficiency decreases with particle multiplicity: $D^0 p\bar{p}$, $K\pi$ is highest at 19% and $D^* p\bar{p}\pi\pi$, $K\pi\pi\pi$ is lowest at $\mathcal{O}(1\%)$; they are given later in Table IIa.

B. Fit method and yields

The signal B yield is extracted by fitting the joint distribution of

$$m_{\text{ES}} = \sqrt{\frac{s}{4} - (\mathbf{P}_B)^2} \quad \text{and} \quad \Delta E = E_B - \sqrt{\frac{s}{4}}, \quad (2)$$

where \sqrt{s} is the e^+e^- center-of-mass (cms) energy and \mathbf{P}_B (E_B) is the B candidate momentum (energy) in the cms. Figure 3 gives $m_{\text{ES}}-\Delta E$ scatter plots for the six B decays that are first observations. A concentration of correctly reconstructed B candidates is visible in the region of m_{ES} and ΔE near the nominal B mass of 5.28 GeV/ c^2 and zero, respectively. The uniform distribution of dots over the entire plane is indicative of the general smoothness of the background events.

A 2-dimensional (2d) probability distribution function (pdf) is used to fit $m_{\text{ES}}-\Delta E$ via the unbinned extended maximum likelihood technique [36]. The 2d pdf is a sum of two components for all B decay modes except for $D^{*0} p\bar{p}\pi$, which requires three. These are denoted as P_S , P_B , and P_P respectively, for the signal, background, and peaking background events. The motivation and description for P_P is given later and continued in Sec. III C. The parameters (yields) associated with the components are Ω_S , Ω_B , and Ω_P (n_S , n_B , and n_P), respectively. Since the fit variables are uncorrelated to a good approximation, each 2d pdf component is written as product of two 1d pdfs. P_S is the product of two functions with a Gaussian core and a power-law tail [37]

written as $P_g(m_{ES}; \Omega_S)P_g(\Delta E; \Omega'_S)$. P_B is the product of a threshold function vanishing at the nominal B mass for m_{ES} and a 2nd-order Chebyshev polynomial of the first kind for ΔE written as $P_t(m_{ES}; \Omega_B)P_c(\Delta E; \Omega'_B)$. P_P for $D^{*0}p\bar{p}\pi$ is written as $P_g(m_{ES}; \Omega_P)P_g(\Delta E; \Omega'_P)$.

The fit window of $5.22 < m_{ES} < 5.30 \text{ GeV}/c^2$ and $|\Delta E| < 50 \text{ MeV}$ provides ample sideband regions because the signal resolution of m_{ES} and ΔE are relatively narrow at 2.2–2.5 MeV/ c^2 and 8–10 MeV, respectively. Signal slice projection plots for m_{ES} are defined to be within 2.5σ of the mean value of ΔE and sideband to be outside 4σ and vice versa for ΔE plots. As an illustration of the fit projection over the entire window, Fig. 4ab(cd) gives projections of the 2d pdf in the signal (sideband) slices. For $B^- \rightarrow D^- p\bar{p}\pi\pi$, corresponding to the scatter plot in Fig. 3c, the good description of background in the sideband slices gives us confidence that it is well modeled in the signal box.

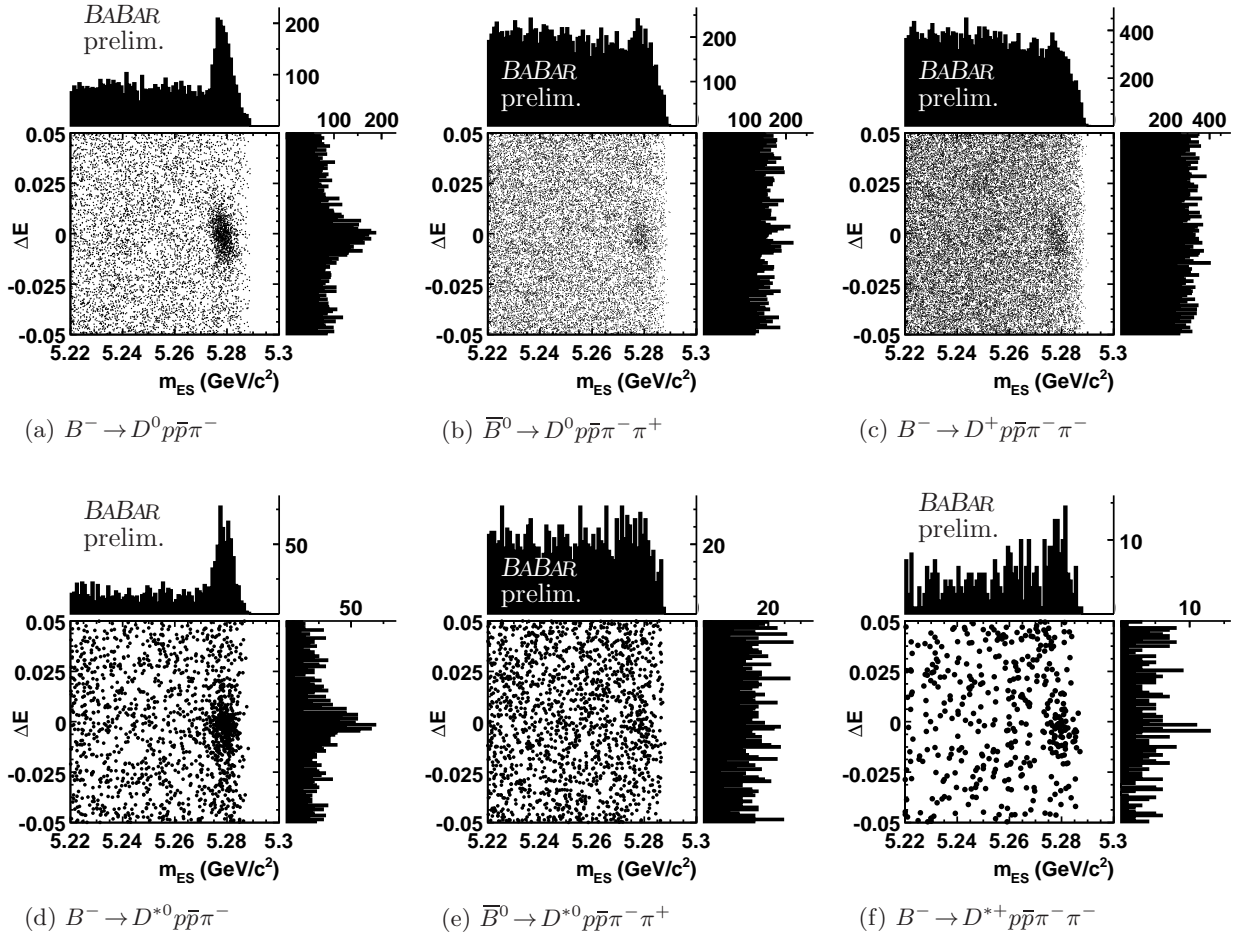


FIG. 3: m_{ES} - ΔE scatter plots for new observations of B decays: (a) $B^- \rightarrow D^0 p\bar{p}\pi$, (b) $\bar{B}^0 \rightarrow D^0 p\bar{p}\pi\pi$, (c) $B^- \rightarrow D^+ p\bar{p}\pi\pi$, (d) $B^- \rightarrow D^{*0} p\bar{p}\pi$, (e) $\bar{B}^0 \rightarrow D^{*0} p\bar{p}\pi\pi$, and (f) $B^- \rightarrow D^{*+} p\bar{p}\pi\pi$. We show the cleanest mode with $D^{0,+} \rightarrow K^- \pi^-$, $K^- \pi^+ \pi^+$, resp. Histograms on top (right) are m_{ES} (ΔE) projections in 1 MeV/ c^2 (MeV) bins; no cut is made on the complementary variable.

The likelihood for N data events is defined as

$$\mathcal{L} = \frac{e^{-(n_S+n_B)}}{N!} \prod_{i=1}^N \left[n_S \underbrace{P_g(m_{ESi}; \Omega_S) P_g(\Delta E_i; \Omega'_S)}_{\text{signal pdf } P_S} + n_B \underbrace{P_t(m_{ESi}; \Omega_B) P_c(\Delta E_i; \Omega'_B)}_{\text{background pdf } P_B} \right], \quad (3)$$

where m_{ESi} and ΔE_i are the values for the i^{th} event. For $D^{*0} p\bar{p}\pi$, we add a third component in Eqn. 3 for peaking background. The quantity $-\ln \mathcal{L}$ is minimized with respect to the parameters and yields using MINUIT [38] via the ROOFIT toolkit [39] in ROOT [40]. We fix some parameters to values obtained in fits to MC distributions. For P_S , these are the Gaussian width and power-law tail parameters; for P_B , the end-point of the threshold pdf for m_{ES} ; and for P_P , all parameters including the the yield n_P using the branching fraction and acceptance found for $D^{*+} p\bar{p}\pi$. To check for possible pathological behaviors in the fit, we perform one thousand mock experiments where events are drawn from the pdf and subsequently fit with the same pdf. All means (widths) of signal yield pull distributions are consistent with zero (unity).

Figs. 5, 6, and 7 give the collection of m_{ES} sliced projections in the ΔE signal region for 3-, 4-, and 5-body B decays, respectively. Signal yields range from 50–3500 events for the ten B decays; they are given later in Table IIa. Lastly, additional work is done for four \bar{B}^0 decay chains $D^{(*)0} p\bar{p}\pi\pi$, $K\pi\pi^0$ and $D^{(*)0} p\bar{p}\pi\pi$, $K\pi\pi\pi$ shown in Fig. 7bcef because the fits converged to non-physical Gaussian mean values for $P_g(m_{ES})$ and $P_g(\Delta E)$ due to the low signal-to-background ratio. For these, the means are fixed to the values found for the $K\pi$ counterpart and the end-point for $P_t(m_{ES})$ is floated. We note that these measurements do not contribute significantly to the branching fraction averaged over D^0 decay modes because of large systematic uncertainties compared to the corresponding $K\pi$ measurement; this will be discussed later in Sec. III C.

C. Systematic studies

Table Ia lists the individual sources of systematic uncertainties for the branching fraction measurement in five categories (I–V): B counting, assumed branching fractions for $\Upsilon(4S)$ and $D^{(*)}$, acceptance, pdf, and peaking background estimate.

I. $B\bar{B}$ is counted by subtracting the total number of hadronic events taken at \sqrt{s} of 10.58 GeV by the expected number due to continuum events, which is estimated using data taken at 10.54 GeV.

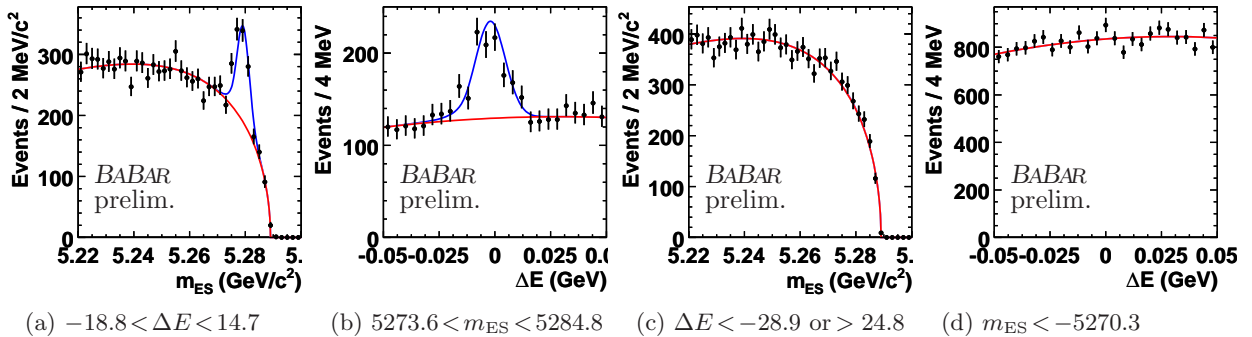


FIG. 4: The m_{ES} - ΔE fit projections for $B^- \rightarrow D^+ p\bar{p}\pi\pi$, $D^+ \rightarrow K\pi\pi$ in (ab) signal and (cd) sideband regions with requirements denoted in the caption in MeV/c^2 (MeV) for m_{ES} (ΔE). For signal slices in (ab), the top blue curve is the signal pdf P_S ; bottom red is the background pdf P_B . For sideband slices in (cd), no part of the signal pdf is present in this region and the background pdf is identical to the corresponding plot in (ab).

The total uncertainty is 1.1% and the largest component comes from the comparison of detection efficiencies of hadronic events in data and MC.

II. We assume equal production of $\Upsilon(4S) \rightarrow B^0 \bar{B}^0$ and $B^+ B^-$ as well as nominal branching fractions for D^* and D . (1) For $\Upsilon(4S)$, we take the absolute difference between the nominal value and 50%, which gives 1.6%. (2) For D^{*0} (D^{*+}), the uncertainties are 4.7% (0.7%). For D , the uncertainties are 1.3%, 3.7%, 2.5%, and 2.3% for $K\pi$, $K\pi\pi^0$, $K\pi\pi\pi$, and $K\pi\pi$, respectively.

III. The reconstruction efficiency has seven contributing sources. (1) Charged track identification uncertainty of 0.5% per track is obtained by comparing data and simulations with $e^+e^- \rightarrow \tau^+\tau^-$ events where one tau decays leptonically and the other tau decays hadronically. (2) Because soft charged pions from D^{*+} decays leave hits only in the silicon vertex tracker, they have an additional uncertainty of 3.1%, which is obtained from using the helicity angle distribution of the decay daughters [41]. (3) Neutral pions identification of 3.0% is obtained by comparing data and MC $\tau^+\tau^-$ events where one tau decays leptonically and the other decay includes a π^0 . (4) Acceptance of signal B decays computed using the MC assuming the uniform phase space decay model is compared with the data distribution in bins of $m^2(p\bar{p})$ and $m^2(D^{(*)}p)$ where the most variation is seen. We obtain uncertainties ranging from 0.8–9.7% with modes containing a D^{*+} at the higher end of the spectrum. (5) Kaon identification uncertainty of 0.5% is obtained by comparing data control samples of $D^0 \rightarrow K\pi$ from inclusively produced $D^* \rightarrow D^0\pi$ and from similar B decays. (6) Proton identification uncertainty of 1% is obtained by comparing various data control samples of inclusively produced $\Lambda \rightarrow p\pi^-$ with decay topologies of high charged-particle multiplicities that mimic our B decay environment. (7) Corrections made for particle identification contribute additional statistical uncertainties that range from 1.5–2.5%.

IV. The fit pdf has four contributing sources. (1) As described in Sec. III, some parameters

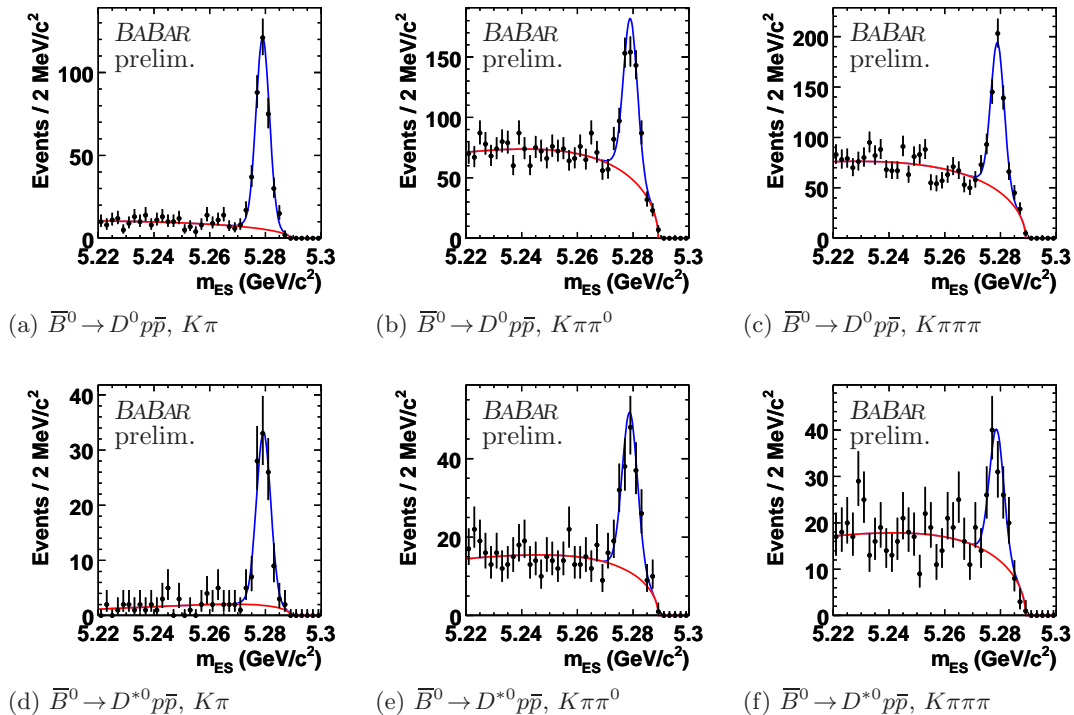


FIG. 5: Fit projections of m_{ES} for 3-body decays (abc) $\bar{B}^0 \rightarrow D^0 p \bar{p}$ and (def) $\bar{B}^0 \rightarrow D^{*0} p \bar{p}$ for each D decay chain. The data sample is a selection of events within 2.5σ of ΔE mean. The pdf is integrated over the said range and the components from the top are P_S in blue and P_B in red.

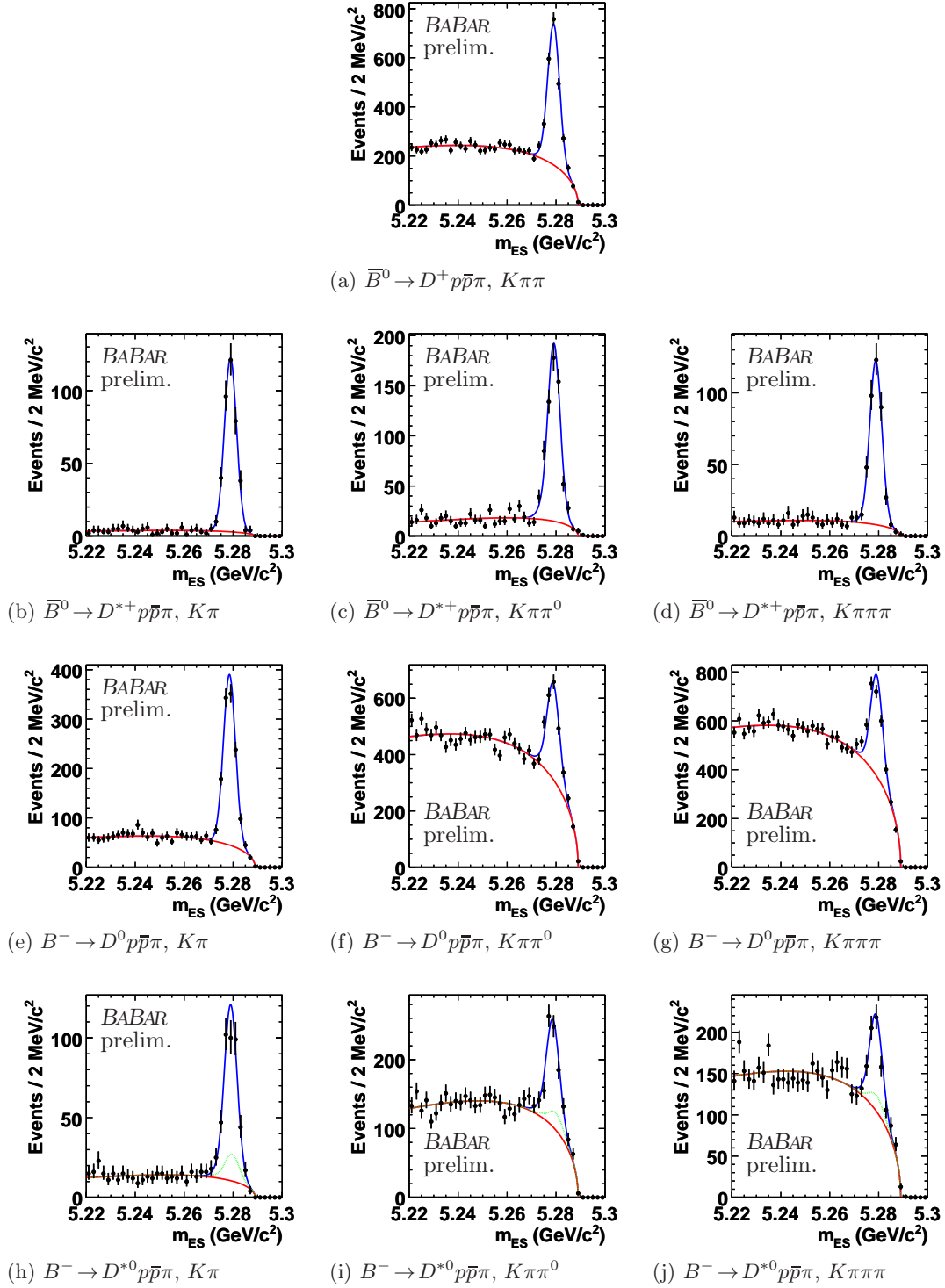


FIG. 6: Fit projections of m_{ES} for 4-body decays (a) $\bar{B}^0 \rightarrow D^+ p\bar{p}\pi^-$, (bcd) $\bar{B}^0 \rightarrow D^{*+} p\bar{p}\pi^-$, (efg) $B^- \rightarrow D^0 p\bar{p}\pi^-$, and (hij) $B^- \rightarrow D^{*0} p\bar{p}\pi^-$ for each D decay chain. The data sample is a selection of events within 2.5σ of ΔE mean. The pdf is integrated over the said range and the components from the top are P_S in blue and P_B in red. For (hij), P_P is the middle pdf in green.

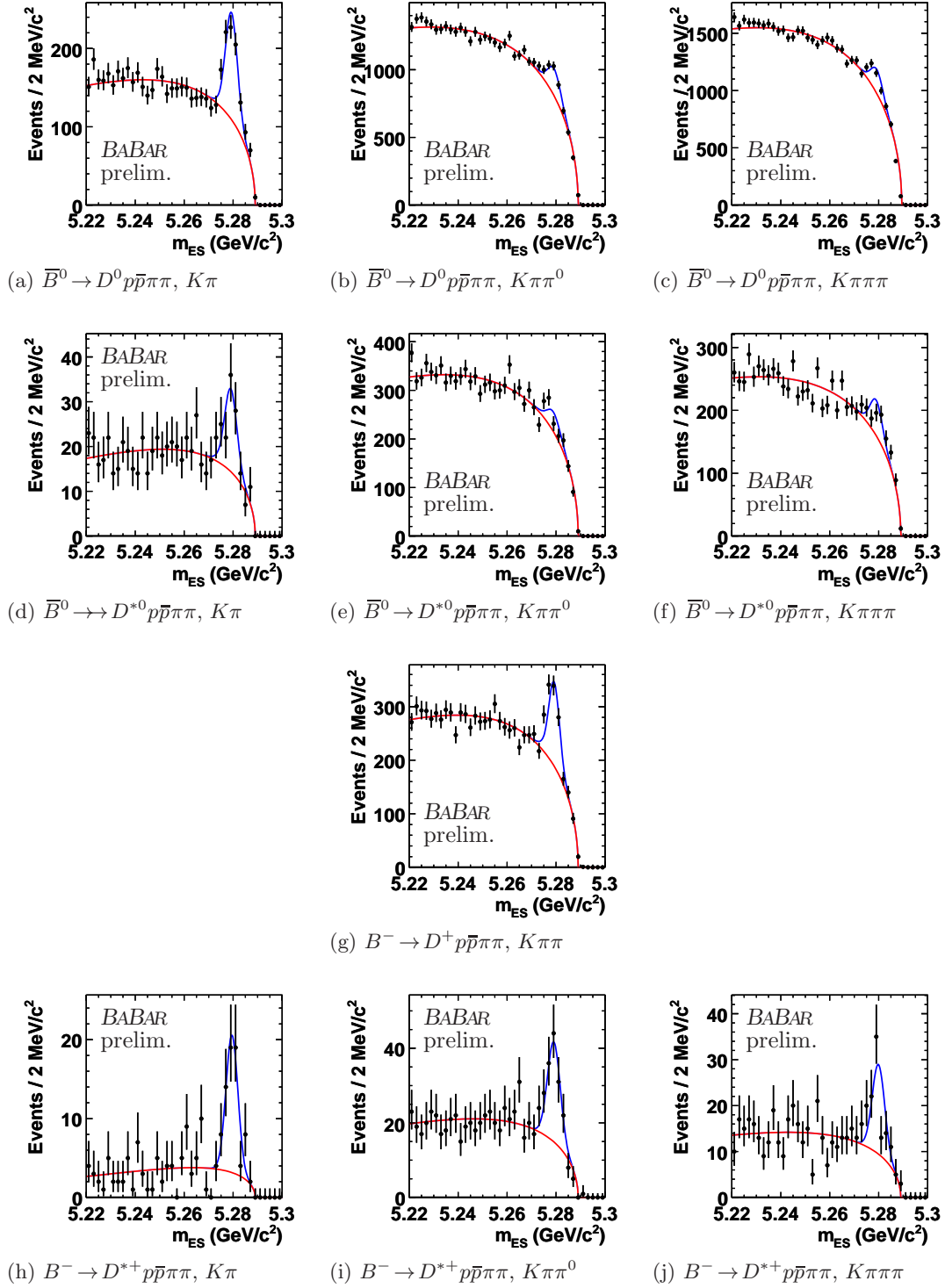


FIG. 7: Fit projections of m_{ES} for 5-body decays (abc) $\bar{B}^0 \rightarrow D^0 p \bar{p} \pi^- \pi^+$, (def) $\bar{B}^0 \rightarrow D^{*+} p \bar{p} \pi^-$, (g) $B^- \rightarrow D^0 p \bar{p} \pi^- \pi^-$, and (hij) $B^- \rightarrow D^{*0} p \bar{p} \pi^- \pi^-$ for each D decay chain. The data sample is a selection of events within 2.5σ of ΔE mean. The pdf is integrated over the said range and the components from the top are P_S in blue and P_B in red.

are fixed to values determined by the MC sample. These are varied by the uncertainties obtained when fitting the MC and the quadrature sum of the typical yield changes are 1.3, 2.8, 5.7, and 3.4% for modes with $D \rightarrow K\pi$, $K\pi\pi^0$, $K\pi\pi\pi$, and $K\pi\pi$, respectively. (2) A more general signal pdf is chosen and the typical yield change is 0.6%. (3) A more general background pdf is chosen and the typical yield changes are 0.8, 4.5, 1.3, and 2.0% for modes with $D \rightarrow K\pi$, $K\pi\pi^0$, $K\pi\pi\pi$, and $K\pi\pi$, respectively. (4) Sec. IIIB described a thousand mock experiments to check for possible pathologies of the pdf. We generalize this study by embedding the MC with signal B decays into background events drawn from the background pdf. Signal yield bias ranges from 0.4–2.2%, which we assign as a systematic uncertainty.

V. Peaking background sources have three contributing sources. (1) Possible sources of events that peak in the signal box around $m_{ES} = 5.28 \text{ GeV}/c^2$ and $\Delta E = 0 \text{ MeV}$ have been studied exten-

TABLE I: Systematic uncertainties for measurements of B branching fractions, \mathcal{B} .

(a) List of individual systematic uncertainties in five categories (I–V).

Item	Source description	% of \mathcal{B}
I	$B\bar{B}$ counting	1.1
II.1	Branching fraction of $\Upsilon(4S)$	1.6
II.2	Branching fraction of $D \rightarrow K\pi$, $K\pi\pi^0$, $K\pi\pi\pi$, $K\pi\pi$	1.8, 4.4, 3.2, 3.6, resp.
II.3	Branching fraction of $D^* \rightarrow D^0\pi^0$, $D^0\pi^+$	4.7, 0.7, resp.
III.1	Efficiency of finding charged tracks not including soft pions	0.5 per track
III.2	Efficiency of finding soft charged pions from D^{*+}	3.1 per π
III.3	Efficiency of finding neutral pions	3.0 per π^0
III.4	Efficiency of finding B decays in bins of $m^2(p\bar{p})$ and $m^2(D^{*}p)$	0.8 to 9.7
III.5	Efficiency of finding kaons in B decays	0.5 per K
III.6	Efficiency of finding protons in B decays	1.0 per p
III.7	Efficiency of particle identification based on data control samples	1.5 to 2.5
IV.1	Pdf parameter variation for modes with $D \rightarrow K\pi$, $K\pi\pi^0$, $K\pi\pi\pi$, $K\pi\pi$	1.3, 2.8, 5.7, 3.4, resp.
IV.2	Pdf choice for signal events	0.6
IV.3	Pdf choice for background events for $D \rightarrow K\pi$, $K\pi\pi^0$, $K\pi\pi\pi$, $K\pi\pi$	0.8, 4.5, 1.3, 2.0, resp.
IV.4	Pdf yield bias by fitting mock experiments embedded with MC	0.4 to 2.2
V.1	Peaking background in $m_{ES}-\Delta E$	8.0 for $D^{*0}p\bar{p}\pi$
V.2	Peaking background in m_{ES} only ($D^{*0}p\bar{p}\pi\pi$, $K\pi\pi^0$ and $D^{*0}p\bar{p}\pi\pi$, $K\pi\pi\pi$)	0.0 to 14.5 (77 to 85)
V.3	Peaking background from identical final states without a D meson	0.5 to 13.5

(b) Uncorrelated sources (% of \mathcal{B})

N -body	D decay				
	B decay	$K\pi$	$K\pi\pi^0$	$K\pi\pi\pi$	$K\pi\pi$
3-body	$\bar{B}^0 \rightarrow D^0 p\bar{p}$	2.7	5.5	4.7	-
"	$\bar{B}^0 \rightarrow D^{*0} p\bar{p}$	2.2	8.6	8.7	-
4-body	$\bar{B}^0 \rightarrow D^+ p\bar{p}\pi^-$	-	-	-	5.7
"	$\bar{B}^0 \rightarrow D^{*+} p\bar{p}\pi^-$	4.2	7.6	9.9	-
"	$B^- \rightarrow D^0 p\bar{p}\pi^-$	14.5	81.2	77.3	-
"	$B^- \rightarrow D^{*0} p\bar{p}\pi^-$	13.8	86.3	85.4	-
5-body	$\bar{B}^0 \rightarrow D^0 p\bar{p}\pi^- \pi^+$	4.4	8.8	11.6	-
"	$\bar{B}^0 \rightarrow D^{*0} p\bar{p}\pi^- \pi^+$	10.4	11.6	13.2	-
"	$B^- \rightarrow D^+ p\bar{p}\pi^- \pi^-$	-	-	-	15.0
"	$B^- \rightarrow D^{*+} p\bar{p}\pi^- \pi^-$	5.9	14.9	19.0	-

(c) Correlated sources excluding II.2, II.3 (% of \mathcal{B})

N -body	D decay				
	B decay	$K\pi$	$K\pi\pi^0$	$K\pi\pi\pi$	$K\pi\pi$
3-body	$\bar{B}^0 \rightarrow D^0 p\bar{p}$	3.5	6.9	7.0	-
"	$\bar{B}^0 \rightarrow D^{*0} p\bar{p}$	4.6	8.6	7.7	-
4-body	$\bar{B}^0 \rightarrow D^+ p\bar{p}\pi^-$	-	-	-	5.6
"	$\bar{B}^0 \rightarrow D^{*+} p\bar{p}\pi^-$	6.3	8.6	8.9	-
"	$B^- \rightarrow D^0 p\bar{p}\pi^-$	3.9	7.0	7.0	-
"	$B^- \rightarrow D^{*0} p\bar{p}\pi^-$	4.9	8.8	7.7	-
5-body	$\bar{B}^0 \rightarrow D^0 p\bar{p}\pi^- \pi^+$	4.2	7.2	7.3	-
"	$\bar{B}^0 \rightarrow D^{*0} p\bar{p}\pi^- \pi^+$	5.2	8.9	7.9	-
"	$B^- \rightarrow D^+ p\bar{p}\pi^- \pi^-$	-	-	-	5.9
"	$B^- \rightarrow D^{*+} p\bar{p}\pi^- \pi^-$	6.8	9.0	9.2	-

sively using a sample of $\mathcal{O}(10^9)$ MC events with B decays hadronized using JETSET 7.4 [30] as well as a sample of $\mathcal{O}(10^8)$ MC events dedicated to a set of B decays to a $D^{(*)}$, a $p\bar{p}$ pair, and a system of up to two charged or neutral pions followed by a comprehensive set of $D^{(*)}$ decays including those not reconstructed in our study. We find only one scenario meeting our requirement: events generated as $\bar{B}^0 \rightarrow D^{*+} p\bar{p}\pi^-$ reconstructed as $B^- \rightarrow D^{*0} p\bar{p}\pi^-$. In this case, we fit the MC and add the pdf component in the fit to data in Eqn. 3 as described in Sec. IIIB. The normalization is the product of the acceptance and branching fraction for $D^{*+} p\bar{p}\pi^-$. The total uncertainty on the latter quantity is 8% and is assigned as a systematic. (2) Possible sources of events that peak either in $m_{ES} = 5.28 \text{ GeV}/c^2$ or in $\Delta E = 0 \text{ MeV}$ have been studied using the above-mentioned set of MC. We find that only a few samples exhibit a peak in m_{ES} that occur when a related decay is misreconstructed by losing or gaining either a π^0 or a γ from the other B decay in the event; we find no cases of events peaking only in ΔE . In the m_{ES} -peaking cases, the distributions peak broadly with a Gaussian width of around $10 \text{ MeV}/c^2$ and has a smooth variation in ΔE . One such distribution is fit and the component is added to our nominal fit in Eqn. 3 as a systematic study. The signal yield changes varied from 0–15% with four exceptions: in the decays $D^{(*)} p\bar{p}\pi\pi$, $K\pi\pi^0$ and $D^{(*)} p\bar{p}\pi\pi$, $K\pi\pi\pi$ shown in Fig. 6bc (6ef), the signal yields varied by 77–85%. This is not surprising because we saw in Sec. IIIB that the fit was not stable against our initial strategy and had to be forced to find a peak at the desired location by fixing the means of P_S . For these four B modes, the $K\pi$ measurement is heavily weighted due to these systematic errors with respect to both $K\pi\pi^0$ and $K\pi\pi\pi$ when we average the B branching fraction over D decay modes. (3) Possible sources of events that share the final states with desired decays are studied by using $m(D)$ sidebands in data. One such example scenario would be $B \rightarrow \Lambda_c \bar{p}\pi^0$, $\Lambda_c \rightarrow pK\pi$ misreconstructed as $\bar{B}^0 \rightarrow D^0 p\bar{p}$, $D^0 \rightarrow K\pi\pi^0$, which would live under the D mass peak in the $m(D)$ distribution. To correct for such a bias, we scale the B signal yield in the $m(D)$ sideband region to the amount of D background in the $m(D)$ signal region. This is given later as a correction factor n_b in Table IIa and the uncertainties range from 0.5–13.5%.

Combining systematic uncertainties requires us to divide uncorrelated sources from those that are not. Table Ib gives the uncorrelated items III.4, III.7, IV.4, V.1, V.2, and V.3 summed in quadrature. Table Ic gives the correlated sources, which are computed in two steps. Correlated sources for the individual decay chains—III.1, 2, 3, and 6—are summed linearly; Correlated sources for B decays—I; II.1; III.5 and 6; and IV.1, 2, and 3—are summed in quadrature. Lastly, the error matrix, \mathbf{V} , is constructed. For decays with a D^0 , \mathbf{V} is a 3×3 matrix spanned by the three decay modes ($K\pi$, $K\pi\pi^0$, $K\pi\pi\pi$) labeled by α and β ; for those with a D^+ , it is a 1×1 matrix for $K\pi\pi$:

$$\begin{aligned}
\mathbf{V} &= \mathbf{V}_{\text{stat}} + \overbrace{\mathbf{V}_{\text{unc}} + \mathbf{V}_{\text{cor}}}^{\mathbf{V}_{\text{syst}}} && \text{is the sum of statistical and systematic components} \\
\mathbf{V}_{\text{stat}} &= \text{diag}[\sigma_{S,\alpha}^2] && \text{for statistical errors from fitting for the signal yield} \\
\mathbf{V}_{\text{unc}} &= \text{diag}[\sigma_{\text{unc},\alpha}^2] && \text{for uncorrelated systematic errors} \\
\mathbf{V}_{\text{cor}} &= \text{diag}[\sigma_{\text{cor},\alpha}^2] + \rho_{\alpha\beta} \sigma_{\text{cor},\alpha} \sigma_{\text{cor},\beta} && \text{for correlated systematic errors,}
\end{aligned} \tag{4}$$

where $\rho_{\alpha\beta}$ is the correlation coefficient and σ_S is given later in Table IIa. The $\rho_{\alpha\beta}$ for D^0 branching fraction are given in [32] and all other coefficients are assumed to be unity.

IV. BRANCHING FRACTIONS

A. Weighted average

Branching fractions are found in two steps: they are computed for 26 decay chains, then averaged over D decay modes. The branching fraction for a B decay followed by $D \rightarrow K\pi$ denoted by α , is

$$\mathcal{B}_\alpha = \frac{1}{N_{B\bar{B}}} \frac{1}{\mathcal{B}(D^* \rightarrow D^0\pi)} \frac{1}{\mathcal{B}(D \rightarrow \alpha)} \frac{1}{\epsilon} (n_S - n_b), \quad (5)$$

where $N_{B\bar{B}} = 455 \times 10^6$, $\mathcal{B}(D^{(*)})$ is the $D^{(*)}$ branching fraction, ϵ is the acceptance, n_S is the signal yield, and n_b is the D -mass-sideband peaking background correction. Branching fractions for eight B decays with a D^0 form a vector $\vec{\mathcal{B}} = (\mathcal{B}_{K\pi}, \mathcal{B}_{K\pi\pi^0}, \mathcal{B}_{K\pi\pi\pi})^T$; for two with a D^+ , $\vec{\mathcal{B}} = (\mathcal{B}_{K\pi\pi})^T$.

Table II presents the branching fractions and their ingredients for the 26 decay chains and the combined values, $\mathcal{B}_{\text{avg}} = \vec{\mathcal{B}} \cdot \vec{w}$, which are averaged over D^0 decay modes using a method [42] to compute the weights from error matrices in Eqn. 4

$$\vec{w} = \frac{\mathbf{V}^{-1} \cdot \vec{u}}{\vec{u}^T \cdot \mathbf{V}^{-1} \cdot \vec{u}}, \quad (6)$$

where $\vec{u} = (1,1,1)^T$. The squared combined statistical uncertainty is $\sigma_{\text{stat}}^2 = \vec{w}^T \cdot \mathbf{V}_{\text{stat}} \cdot \vec{w}$ and similarly computed for systematics. All measurements are statistically significant.

For B decays with a D^0 meson, consistency between the three measurements is evaluated by $\chi^2 = (\vec{\mathcal{B}} - \mathcal{B}_{\text{avg}}\vec{u})^T \cdot \mathbf{V}^{-1} \cdot (\vec{\mathcal{B}} - \mathcal{B}_{\text{avg}}\vec{u})$ and the associated probability $P(\chi^2) = \exp[-\chi^2/2]/2$. For all cases, $P(\chi^2)$ is greater than 10%.

B. Ratios

Tables III gives ratios of branching fractions that show two general patterns. First, the ratios are of order unity for modes related by replacing D mesons. The unit ratio for $D \leftrightarrow D^*$ replacement suggests that the additional D^* polarization degrees of freedom does not increase production. The unit ratio for $D^{(*)+} \leftrightarrow D^{(*)0}$ suggests that the production can be described by simple isospin relations. Second, the ratios for modes related by addition of pions imply the hierarchy of $\mathcal{B}_{3\text{-body}} < \mathcal{B}_{5\text{-body}} < \mathcal{B}_{4\text{-body}}$.

V. DECAY DYNAMICS

A. Three-body decays $B \rightarrow D^{(*)} p\bar{p}$

Figure 8 gives the Dalitz plot for 3-body B decay modes, where we sum over D^0 decays. Each point in the $m^2(p\bar{p})$ - $m^2(D^{(*)0}p)$ plane represents an event and we observe threshold enhancements in both variables.¹ Red lines are drawn as visual guides: the threshold effect in $p\bar{p}$ ($D^{(*)0}p$) is on the left (bottom) of the vertical (horizontal) line at 5 (9) GeV^2/c^4 . The two regions do not overlap.

We investigate the enhancements with mass projection plots using the background subtraction technique [43] by weighting pdf components and associated yields, which were described in Eqn. 3

¹ B candidates are refit with the B -mass constraint so that events lie in the region allowed by kinematic limits.

TABLE II: B branching fractions, \mathcal{B} , (a) for 26 decay chains and (b) averaged over D modes.

 (a) \mathcal{B} and its ingredients. See Eqn. 5.

N -body	B decay chain	$n_S \pm \sigma_S$	n_b	ϵ (%)	\mathcal{B}_D (%)	\mathcal{B}_{D^*} (%)	$\mathcal{B} \pm \sigma_{\text{stat}}$ (10^{-4})
3-body	$\bar{B}^0 \rightarrow D^0 p \bar{p}, K\pi$	351 ± 20	7.6	19.04	3.89	-	1.02 ± 0.06
"	$\bar{B}^0 \rightarrow D^0 p \bar{p}, K\pi\pi^0$	$431 \pm \frac{28}{27}$	23.7	7.01	13.5	-	0.95 ± 0.06
"	$\bar{B}^0 \rightarrow D^0 p \bar{p}, K\pi\pi\pi$	$448 \pm \frac{27}{26}$	10.1	9.85	8.10	-	1.21 ± 0.07
"	$\bar{B}^0 \rightarrow D^{*0} p \bar{p}, D^0\pi, K\pi$	$110 \pm \frac{12}{11}$	-1.4	9.40	3.89	61.9	1.08 ± 0.12
"	$\bar{B}^0 \rightarrow D^{*0} p \bar{p}, D^0\pi, K\pi\pi^0$	148 ± 15	3.9	3.24	13.5	61.9	1.17 ± 0.12
"	$\bar{B}^0 \rightarrow D^{*0} p \bar{p}, D^0\pi, K\pi\pi\pi$	$95 \pm \frac{14}{13}$	5.5	5.15	8.10	61.9	0.76 ± 0.12
4-body	$\bar{B}^0 \rightarrow D^+ p \bar{p}\pi, K\pi\pi$	$1816 \pm \frac{53}{52}$	55.2	12.64	9.22	-	3.32 ± 0.10
"	$\bar{B}^0 \rightarrow D^{*+} p \bar{p}\pi, D^0\pi, K\pi$	$392 \pm \frac{21}{20}$	2.3	6.79	3.89	67.7	4.79 ± 0.26
"	$\bar{B}^0 \rightarrow D^{*+} p \bar{p}\pi, D^0\pi, K\pi\pi^0$	$601 \pm \frac{28}{27}$	20.7	3.08	13.5	67.7	4.53 ± 0.22
"	$\bar{B}^0 \rightarrow D^{*+} p \bar{p}\pi, D^0\pi, K\pi\pi\pi$	$378 \pm \frac{22}{21}$	19.9	3.66	8.10	67.7	3.92 ± 0.24
"	$B^- \rightarrow D^0 p \bar{p}\pi, K\pi$	$1078 \pm \frac{38}{37}$	13.1	15.89	3.89	-	3.79 ± 0.14
"	$B^- \rightarrow D^0 p \bar{p}\pi, K\pi\pi^0$	$1176 \pm \frac{54}{53}$	41.1	5.53	13.5	-	3.34 ± 0.16
"	$B^- \rightarrow D^0 p \bar{p}\pi, K\pi\pi\pi$	$1296 \pm \frac{57}{56}$	33.0	7.82	8.10	-	4.38 ± 0.20
"	$B^- \rightarrow D^{*0} p \bar{p}\pi, D^0\pi, K\pi$	328 ± 22	2.1	7.71	3.89	61.9	3.86 ± 0.26
"	$B^- \rightarrow D^{*0} p \bar{p}\pi, D^0\pi, K\pi\pi^0$	$482 \pm \frac{35}{34}$	46.5	2.87	13.5	61.9	3.99 ± 0.32
"	$B^- \rightarrow D^{*0} p \bar{p}\pi, D^0\pi, K\pi\pi\pi$	$343 \pm \frac{31}{30}$	32.4	4.04	8.10	61.9	3.37 ± 0.34
5-body	$\bar{B}^0 \rightarrow D^0 p \bar{p}\pi\pi, K\pi$	$438 \pm \frac{32}{31}$	7.7	8.19	3.89	-	2.97 ± 0.22
"	$\bar{B}^0 \rightarrow D^0 p \bar{p}\pi\pi, K\pi\pi^0$	$663 \pm \frac{65}{64}$	155.2	2.92	13.5	-	2.83 ± 0.36
"	$\bar{B}^0 \rightarrow D^0 p \bar{p}\pi\pi, K\pi\pi\pi$	$770 \pm \frac{68}{67}$	39.7	3.75	8.10	-	5.28 ± 0.48
"	$\bar{B}^0 \rightarrow D^{*0} p \bar{p}\pi\pi, D^0\pi, K\pi$	61 ± 12	1.8	2.89	3.89	61.9	1.87 ± 0.38
"	$\bar{B}^0 \rightarrow D^{*0} p \bar{p}\pi\pi, D^0\pi, K\pi\pi^0$	$142 \pm \frac{33}{31}$	36.7	1.27	13.5	61.9	2.19 ± 0.66
"	$\bar{B}^0 \rightarrow D^{*0} p \bar{p}\pi\pi, D^0\pi, K\pi\pi\pi$	$163 \pm \frac{30}{29}$	12.8	1.33	8.10	61.9	4.93 ± 0.99
"	$B^- \rightarrow D^+ p \bar{p}\pi\pi, K\pi\pi$	$475 \pm \frac{37}{36}$	6.6	6.74	9.22	-	1.66 ± 0.13
"	$B^- \rightarrow D^{*+} p \bar{p}\pi\pi, D^0\pi, K\pi$	57 ± 9	-12.4	2.93	3.89	67.7	1.98 ± 0.26
"	$B^- \rightarrow D^{*+} p \bar{p}\pi\pi, D^0\pi, K\pi\pi^0$	$94 \pm \frac{14}{13}$	-0.6	1.25	13.5	67.7	1.82 ± 0.27
"	$B^- \rightarrow D^{*+} p \bar{p}\pi\pi, D^0\pi, K\pi\pi\pi$	$66 \pm \frac{12}{11}$	4.8	1.52	8.10	67.7	1.61 ± 0.32

 (b) \mathcal{B} averaged over D decay modes and previous measurements [9, 11, 13] in units of (10^{-4}). See Eqn. 6.

N -body	B decay	$\mathcal{B} \pm \sigma_{\text{stat}} \pm \sigma_{\text{syst}}$	χ^2	$P(\chi^2)$	Refs. [9, 11]	Ref. [13]
3-body	$\bar{B}^0 \rightarrow D^0 p \bar{p}$	$1.02 \pm 0.04 \pm 0.05$	4.3	12%	$1.18 \pm 0.15 \pm 0.16$ [11]	$1.13 \pm 0.06 \pm 0.08$
"	$\bar{B}^0 \rightarrow D^{*0} p \bar{p}$	$0.97 \pm 0.07 \pm 0.09$	4.1	13%	$1.20 \pm 0.33 \pm 0.21$ [11]	$1.01 \pm 0.10 \pm 0.09$
4-body	$\bar{B}^0 \rightarrow D^+ p \bar{p}\pi^-$	$3.32 \pm 0.10 \pm 0.27$	-	-	-	$3.38 \pm 0.14 \pm 0.29$
"	$\bar{B}^0 \rightarrow D^{*+} p \bar{p}\pi^-$	$4.55 \pm 0.16 \pm 0.37$	1.2	54%	$6.5 \pm 1.3 \pm 1.0$ [9]	$4.81 \pm 0.22 \pm 0.44$
"	$B^- \rightarrow D^0 p \bar{p}\pi^-$	$3.72 \pm 0.11 \pm 0.23$	3.4	19%	-	-
"	$B^- \rightarrow D^{*0} p \bar{p}\pi^-$	$3.73 \pm 0.17 \pm 0.39$	0.5	79%	-	-
5-body	$\bar{B}^0 \rightarrow D^0 p \bar{p}\pi^- \pi^+$	$2.99 \pm 0.21 \pm 0.44$	0.3	85%	-	-
"	$\bar{B}^0 \rightarrow D^{*0} p \bar{p}\pi^- \pi^+$	$1.91 \pm 0.36 \pm 0.29$	0.5	78%	-	-
"	$B^- \rightarrow D^+ p \bar{p}\pi^- \pi^-$	$1.66 \pm 0.13 \pm 0.27$	-	-	-	-
"	$B^- \rightarrow D^{*+} p \bar{p}\pi^- \pi^-$	$1.86 \pm 0.16 \pm 0.18$	0.2	91%	-	-

and given in Table IIa. The weight for the i^{th} event, where $y_i = (m_{\text{ES}i}, \Delta E_i)$, is

$$W_i = \frac{C_{SS}P_S(y_i) + C_{SB}P_B(y_i)}{n_S P_S(y_i) + n_B P_B(y_i)} \quad \text{and} \quad (C_{S\Lambda})^{-1} = \sum_{j=1}^{N \text{ events}} \frac{P_S(y_j)P_\Lambda(y_j)}{(n_S P_S(y_j) + n_B P_B(y_j))^2}, \quad (7)$$

where $\Lambda = S, B$ and C_{SB} quantifies the correlation between the signal and background yields.

Figure 9 shows the differential branching fractions for $p\bar{p}$ and $D^{(*)0}p$ in different regions of the complementary variable, which are found by substituting W_i for $n_S - n_b$ in Eqn. 5 and computing ϵ for the appropriate region binned in the two variables. In general, the distributions for $D^0 p\bar{p}$ and $D^{*0} p\bar{p}$ are similar. One exception is the comparison of $D^{(*)}p$ in the region $m^2(p\bar{p}) > 5 \text{ GeV}^2/c^4$ shown in Fig. 9b and f, where two broad peaks around $100 \text{ MeV}/c^2$ wide are seen for $D^0 p\bar{p}$ at 2.9 and $3.2 \text{ GeV}/c^2$, but only one is seen in $D^{*0} p\bar{p}$ near threshold.

Lastly, we consider the possibility that the $D^0 p$ threshold effect in $\bar{B}^0 \rightarrow D^0 p\bar{p}$ may be due to one or both of two Λ_c states observed [44] at 2.94 and $2.88 \text{ GeV}/c^2$ with a full width of 18 and $6 \text{ MeV}/c^2$, respectively. These states would span 1–2 bins in Fig. 9b and are not sufficient to describe the $150\text{--}200 \text{ MeV}/c^2$ wide enhancement.

B. Four-body decays $B \rightarrow D^{(*)} p\bar{p}\pi$

Figure 10 shows the differential branching fractions for four mass variables for 4-body B decays: $p\bar{p}$, $D^{(*)}p$, $D^{(*)}\bar{p}$, and $p\pi^-$. In $p\bar{p}$, Figs. 10aeim, we see an enhancement production near threshold compared to the phase space expectations. In $D^{(*)}\bar{p}$, Figs. 10bfjn, we see no obvious hints of a narrow exotic 5-quark state around $3.1 \text{ GeV}/c^2$ [45]. In $D^{(*)}p$, Figs. 10egko, the broad threshold structure seen 3-body decays seems to be absent, except perhaps in Fig. 10k for $B^- \rightarrow D^0 p\bar{p}\pi^-$. In $p\pi^-$, Figs. 10dhlp, we observe a narrow structure near $1.5 \text{ GeV}/c^2$, especially in Fig. 10d for $\bar{B}^0 \rightarrow D^+ p\bar{p}\pi^-$, which refer to as X in subsequent discussions.

To investigate X further, we show opposite-sign and same-sign $p\pi$ in finer bins of $10 \text{ MeV}/c^2$

TABLE III: Ratios of branching fractions, r . The σ_{tot} is the quadrature sum of σ_{stat} and σ_{sys} .

(a) Modes related by s - and d -wave $D^{(*)}$ mesons			(b) Modes related by charged and neutral $D^{(*)}$ mesons		
Quantity		$r \pm \sigma_{\text{tot}}$ (σ_{stat})	Quantity		$r \pm \sigma_{\text{tot}}$ (σ_{stat})
$\mathcal{B}_{D^{*0}p\bar{p}}$	$/\mathcal{B}_{D^0p\bar{p}}$	0.95 ± 0.13 (0.08)	$\mathcal{B}_{D^0p\bar{p}\pi}$	$/\mathcal{B}_{D^+p\bar{p}\pi}$	1.12 ± 0.12 (0.05)
$\mathcal{B}_{D^{*+}p\bar{p}\pi}$	$/\mathcal{B}_{D^+p\bar{p}\pi}$	1.37 ± 0.17 (0.06)	$\mathcal{B}_{D^{*0}p\bar{p}\pi}$	$/\mathcal{B}_{D^{*+}p\bar{p}\pi}$	0.82 ± 0.12 (0.05)
$\mathcal{B}_{D^{*0}p\bar{p}\pi}$	$/\mathcal{B}_{D^0p\bar{p}\pi}$	1.00 ± 0.13 (0.05)	$\mathcal{B}_{D^0p\bar{p}\pi\pi}$	$/\mathcal{B}_{D^+p\bar{p}\pi\pi}$	1.80 ± 0.44 (0.19)
$\mathcal{B}_{D^{*0}p\bar{p}\pi\pi}$	$/\mathcal{B}_{D^0p\bar{p}\pi\pi}$	0.64 ± 0.19 (0.13)	$\mathcal{B}_{D^{*0}p\bar{p}\pi\pi}$	$/\mathcal{B}_{D^{*+}p\bar{p}\pi\pi}$	1.03 ± 0.28 (0.21)
$\mathcal{B}_{D^{*+}p\bar{p}\pi\pi}$	$/\mathcal{B}_{D^+p\bar{p}\pi\pi}$	1.12 ± 0.25 (0.13)	Average with χ^2 of 6.6/3		1.00 ± 0.08
Average with χ^2 of 8.9/4		1.01 ± 0.07			
(c) Comparison of 3- to 4-body B decay			(d) Comparison of 4- to 5-body B decay		
Quantity		$r \pm \sigma_{\text{tot}}$ (σ_{stat})	Quantity		$r \pm \sigma_{\text{tot}}$ (σ_{stat})
$\mathcal{B}_{D^{*0}p\bar{p}\pi}$	$/\mathcal{B}_{D^{*0}p\bar{p}}$	3.66 ± 0.48 (0.22)	$\mathcal{B}_{D^+p\bar{p}\pi\pi}$	$/\mathcal{B}_{D^+p\bar{p}\pi}$	0.50 ± 0.10 (0.04)
$\mathcal{B}_{D^0p\bar{p}\pi}$	$/\mathcal{B}_{D^0p\bar{p}}$	3.08 ± 0.62 (0.31)	$\mathcal{B}_{D^{*+}p\bar{p}\pi\pi}$	$/\mathcal{B}_{D^{*+}p\bar{p}\pi}$	0.41 ± 0.06 (0.04)
Average with χ^2 of 0.5/1		3.44 ± 0.38	$\mathcal{B}_{D^0p\bar{p}\pi\pi}$	$/\mathcal{B}_{D^0p\bar{p}\pi}$	0.80 ± 0.14 (0.06)
			$\mathcal{B}_{D^{*0}p\bar{p}\pi\pi}$	$/\mathcal{B}_{D^{*0}p\bar{p}\pi}$	0.51 ± 0.14 (0.10)
			Average with χ^2 of 6.5/3		0.49 ± 0.05

in Figs. 11 and 12 for the two neutral and charged B decay modes, respectively. (The detector resolution around $1.5 \text{ GeV}/c^2$ is less than $4 \text{ MeV}/c^2$.) In Figs. 11ac and 12ac showing opposite-sign $p\pi^-$, the points with error bars show the total number of events in the $m_{\text{ES}}-\Delta E$ signal box, which includes of three components: the B signal without X , the B signal with X , and the non-signal events. Although we do not have any way a priori to determine the first component (B signal without X) a reasonable procedure, which we adopt, is to take the smoothed histogram pdf from the same-sign mass combination of $\bar{p}\pi^-$ in the same B decay mode written as P_{ss} . This procedure has a systematic uncertainty that is difficult to quantify, because the formation of p and \bar{p} is not necessarily symmetric with respect to the π^- in the $B \rightarrow D^{(*)}p\bar{p}\pi^-$ decays. The distribution of $\bar{p}\pi^-$ events as well as the histogram pdf are shown in Figs. 11bd and 12bd. The second component (the B signal with X) is described by a Breit-Wigner line shape written as P_{bw} . The third component

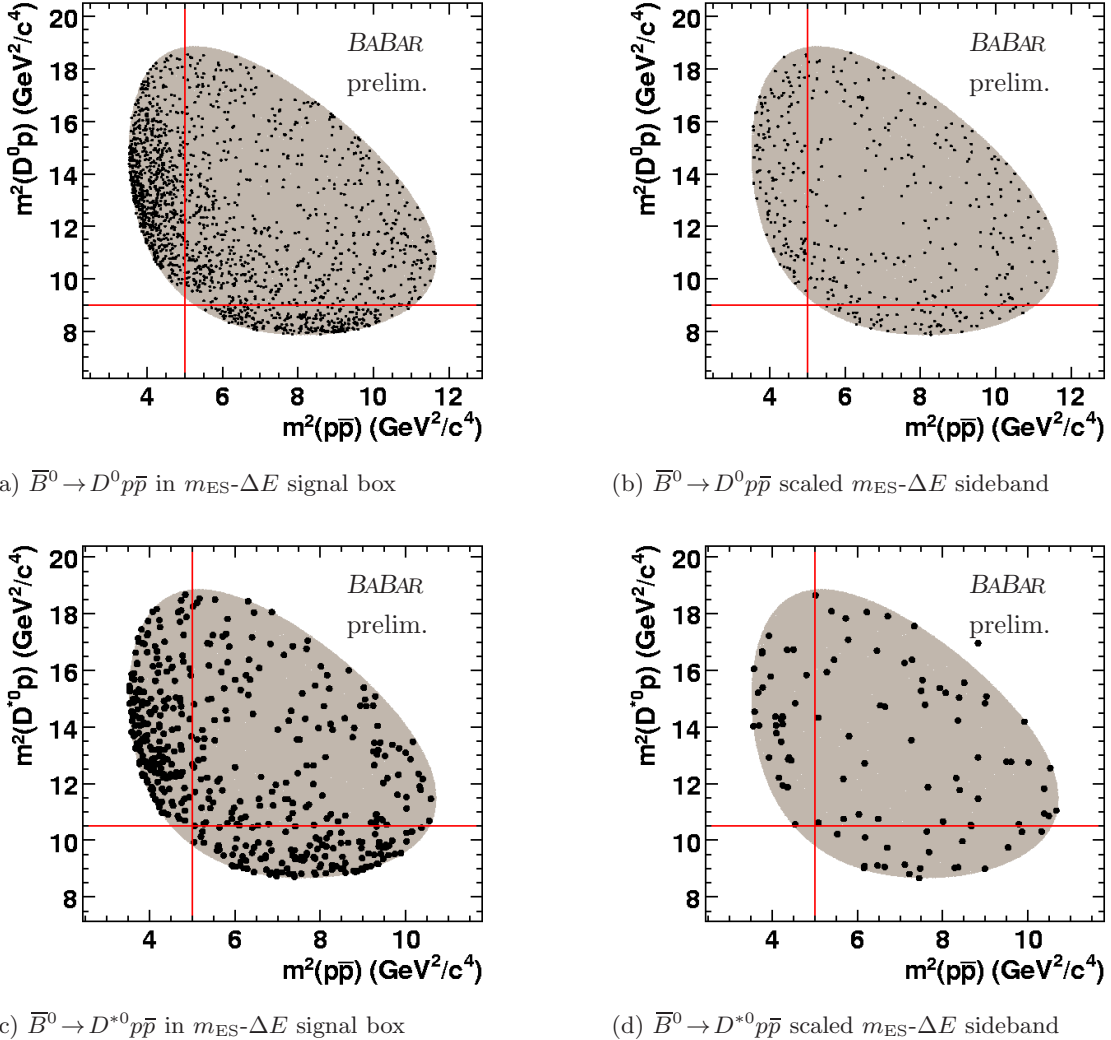


FIG. 8: Dalitz plots of $m^2(p\bar{p})$ vs. $m^2(D^{(*)}p)$ for two 3-body B decays. Plot in (a) shows $\bar{B}^0 \rightarrow D^0 p\bar{p}$ in the $m_{\text{ES}}-\Delta E$ signal box and (b) the sideband region with the number of events corresponding to the background yield in (a). Corresponding plots for $\bar{B}^0 \rightarrow D^{*0} p\bar{p}$ are given in (c) and (d), respectively. Events live in the shaded allowed kinematic region except for one outlier in (d), which failed the re-fit procedure described in footnote d. Red lines are drawn at (x, y) of $(5 \text{ GeV}^2/c^4, 9 \text{ GeV}^2/c^4)$ for (ab) and $(5 \text{ GeV}^2/c^4, 11.5 \text{ GeV}^2/c^4)$ for (cd).

(the non-signal background) can be determined from the $m_{ES}-\Delta E$ sidebands scaled to the number of non-signal events in the signal box. The scaled sideband event samples is shown in Figs. 11–13 as a grey-shaded histogram and we note that these are smooth across region around $1.5 \text{ GeV}/c^2$.

Figures 11a and 11c show the fits of $p\pi^-$ for $\bar{B}^0 \rightarrow D^+ p\bar{p}\pi^-$ and $\bar{B}^0 \rightarrow D^{*+} p\bar{p}\pi^-$, respectively, using P_{bw} and P_{ss} . P_{ss} is relatively flat across X in Figs. 11b and provides a good description of non- X in 11a. However, P_{ss} from Fig. 11d is not as smooth around the signal region and shows a dip just below $1.5 \text{ GeV}/c^2$. We have not yet tried to quantify the uncertainty on this shape. The fit results for $D^+ p\bar{p}\pi^-$ and $D^{*+} p\bar{p}\pi^-$ converged to a mean (width) of 1494.4 ± 4.1 (51 ± 18) MeV/c^2 and 1500.8 ± 4.4 (43 ± 17) MeV/c^2 , respectively, where the errors are statistical. We note a small excess of events above $1.6 \text{ GeV}/c^2$ with respect to P_{ss} , but have not attempted to fit it. The statistical significance of X in $D^+ p\bar{p}\pi^-$ and $D^{*+} p\bar{p}\pi^-$ is found by comparing the likelihood values of our nominal fit to the background-only hypothesis, $\sqrt{2(\ln \mathcal{L}_{bw+ss} - \ln \mathcal{L}_{ss})}$, which is 8.6 and 6.9 standard deviations, respectively, under these background assumptions.

Figures 12a and 12c show the fit to $p\pi^-$ for $B^- \rightarrow D^0 p\bar{p}\pi^-$ and $B^- \rightarrow D^{*0} p\bar{p}\pi^-$, respectively. The above analysis is repeated, but the signals for X in these modes are not as clear compared to the neutral B decays. Moreover, the fit did not converge for $B^- \rightarrow D^0 p\bar{p}\pi^-$ following the procedure, so we re-fit with the X width fixed to the value found for $\bar{B}^0 \rightarrow D^+ p\bar{p}\pi^-$. The fit results are consistent with the values found for neutral B decays, but we leave them out in the average.

Figure 13 shows alternate fits to $p\pi^-$ in $\bar{B}^0 \rightarrow D^+ p\bar{p}\pi^-$. The first, Fig. 13a, uses known excited nucleon resonances at 1440, 1520, 1535, and 1650 MeV/c^2 . The Breit-Wigner parameters are fixed to their nominal values and are written as P_{N^*} . The fit with P_{ss} and P_{N^*} does not well describe the data around $1.5 \text{ GeV}/c^2$. The second, Fig. 13b, uses P_{bw} , P_{ss} , and P'_{ss} , where the last component is the same-sign $\bar{p}\pi^-$ distribution from $\bar{B}^0 \rightarrow D^{*+} p\bar{p}\pi^-$. This is used to determine

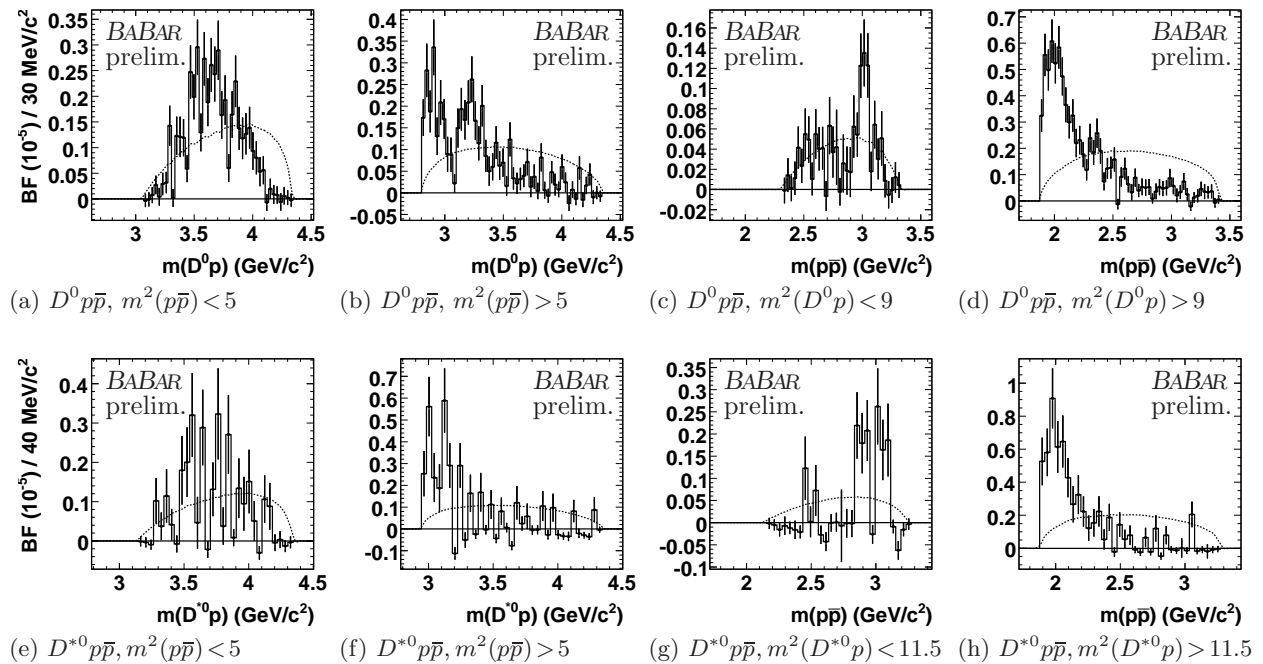


FIG. 9: 3-body B decay mass projection plots for (abcd) $\bar{B}^0 \rightarrow D^0 p\bar{p}$ and (efgh) $\bar{B}^0 \rightarrow D^{*0} p\bar{p}$. Fig. (abef) gives plots of $m(D^{(*)}p)$ in the regions to the left and right of the vertical red line in Fig. 8ab; Fig. (cdgh) plots of $m(p\bar{p})$ above and below the horizontal red line. The curve represents decays following the uniform phase space model. All requirements are given in GeV^2/c^4 .

the systematic uncertainty for our choice of the background pdf, which shifted the mean (width) by 0.8 (4) MeV/ c^2 . Lastly, for the mass uncertainty, we add another 0.5 MeV/ c^2 to the absolute uncertainty due to the variation in the assumed magnetic field and the detector material based on the study of Λ_c [46].

Table IV summarizes the results for X , which can be described by a Breit-Wigner with

$$\begin{aligned} m_X &= (1497.4 \pm 3.0 \pm 0.9) \text{ MeV}/c^2 \\ \Gamma_X &= (47 \pm 12 \pm 4) \text{ MeV}/c^2, \end{aligned} \quad (8)$$

where the errors are statistical and systematic, respectively. The X yields can be compared with the total B yields and their ratios range from 5–15%.

C. Five-body decays $B \rightarrow D^{(*)} p \bar{p} \pi \pi$

Figure 14 shows the differential branching fractions for a selection of four mass variables for 5-body B decays: $p \bar{p}$, $D^{(*)} p$, $D^{(*)} \bar{p}$, and $p \pi^-$. In contrast to 3- and 4-body distributions, we see do not see wide disagreement with phase space expectations.

VI. CONCLUSIONS

Using *BABAR*'s data set of 455×10^6 $B \bar{B}$ pairs, we present the observation and study of ten baryonic B -meson decays to a $D^{(*)}$, a proton-antiproton pair, and a system of up to two pions, of which six ($B^- \rightarrow D^0 p \bar{p} \pi^-$, $B^- \rightarrow D^{*0} p \bar{p} \pi^-$, $\bar{B}^0 \rightarrow D^0 p \bar{p} \pi^- \pi^+$, $\bar{B}^0 \rightarrow D^{*0} p \bar{p} \pi^- \pi^+$, $B^- \rightarrow D^+ p \bar{p} \pi^- \pi^-$, $B^- \rightarrow D^{*+} p \bar{p} \pi^- \pi^-$) are first observations. The branching fractions for 3- and 5-body decays are suppressed compared to 4-body decays with the hierarchy $\mathcal{B}_{3\text{-body}} < \mathcal{B}_{5\text{-body}} < \mathcal{B}_{4\text{-body}}$. Branching fraction ratios for modes related by exchange of D mesons are of order unity.

The kinematic distributions show a number of peculiar features in the B sample. For 3-body decays, non-overlapping threshold enhancements are seen in $m(p \bar{p})$ and $m(D^{(*)0} p)$. For 4-body decays, $m(p \pi^-)$ distribution shows a narrow peak with mass of $(1497.4 \pm 3.0 \pm 0.9) \text{ MeV}/c^2$ and full width of $(47 \pm 12 \pm 4) \text{ MeV}/c^2$, where the first (second) errors are statistical (systematic). For 5-body decays, in contrast to 3- and 4-body decays, mass projections are similar with phase space expectations.

All results are preliminary.

TABLE IV: Fit results of X near 1.5 GeV/ c^2 in $m(p \pi^-)$ for 4-body B decays. The X yield is n_X ; ratio is $r_X = n_X/n_S$ where the B yield is from Table IIa. The fit assumes the same-sign $m(\bar{p} \pi^-)$ combination as the background pdf. All errors are statistical.

Decay	Mean (MeV/ c^2)	Full width (MeV/ c^2)	$\sqrt{2} \Delta \ln \mathcal{L}$	Yield n_X	Ratio r_X (%)
(a) $\bar{B}^0 \rightarrow D^+ p \bar{p} \pi^-$	1494.4 \pm 4.1	51 \pm 18	8.6	227 \pm 51	12.5 \pm 2.8
(b) $\bar{B}^0 \rightarrow D^{*+} p \bar{p} \pi^-$	1500.8 \pm 4.4	43 \pm 17	6.9	120 \pm 31	8.8 \pm 2.3
(c) $B^- \rightarrow D^0 p \bar{p} \pi^-$	1498.8 \pm 6.2	51, fixed to (a)	4.2	183 \pm 45	5.2 \pm 1.3
(d) $B^- \rightarrow D^{*0} p \bar{p} \pi^-$	1495.2 \pm 8.1	71 \pm 34	5.5	169 \pm 59	14.7 \pm 5.1
Stat. average of (a) and (b)	1497.4 \pm 3.0	47 \pm 12	11	-	-

VII. ACKNOWLEDGMENTS

We are grateful for the extraordinary contributions of our PEP-II colleagues in achieving the excellent luminosity and machine conditions that have made this work possible. The success of this

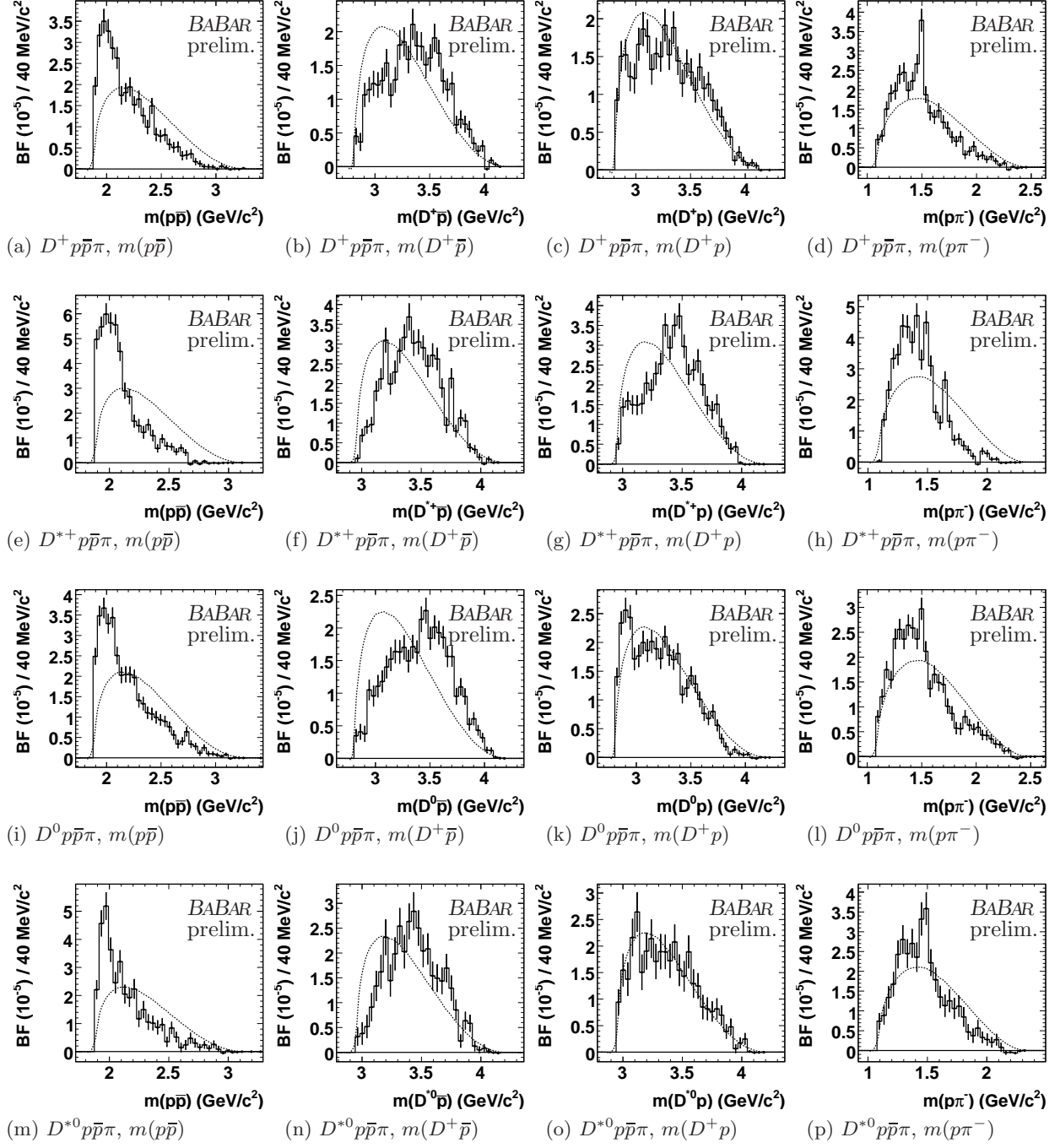
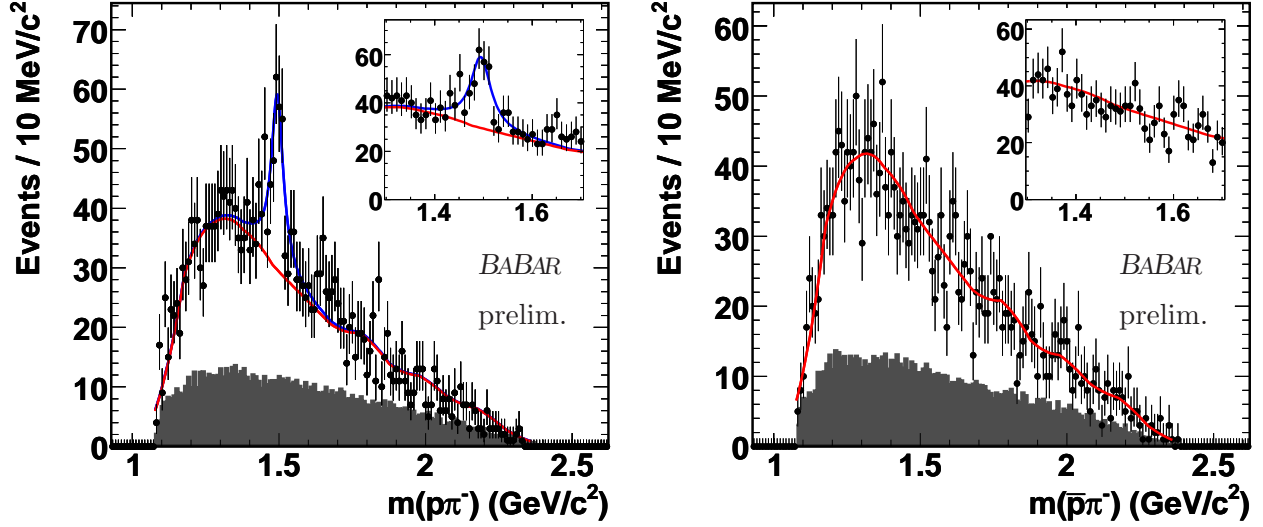


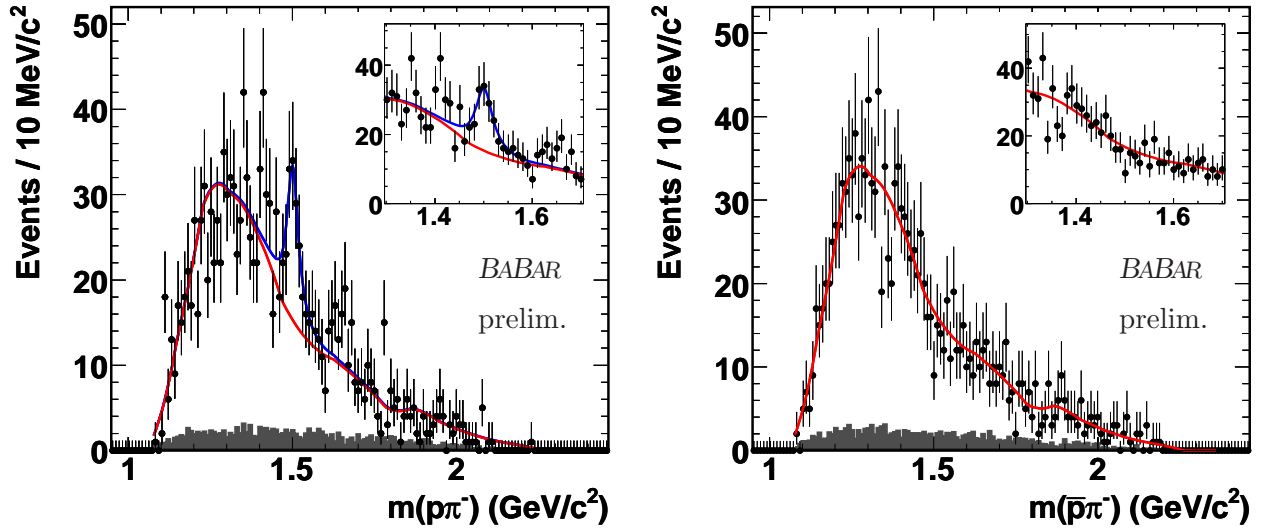
FIG. 10: 4-body B decay differential branching fractions as functions of $p\bar{p}$, $D^{(*)}p$, $D^{(*)}\bar{p}$, and $p\pi^-$ in (abcd) $\bar{B}^0 \rightarrow D^+ p\bar{p}\pi^-$, (efgh) $\bar{B}^0 \rightarrow D^{*+} p\bar{p}\pi^-$, (ijkl) $B^- \rightarrow D^0 p\bar{p}\pi^-$, and (mnop) $B^- \rightarrow D^{*0} p\bar{p}\pi^-$, respectively. The smooth curve represents decays following the uniform phase space model.

project also relies critically on the expertise and dedication of the computing organizations that support *BABAR*. The collaborating institutions wish to thank SLAC for its support and the kind hospitality extended to them. This work is supported by the US Department of Energy and National Science Foundation, the Natural Sciences and Engineering Research Council (Canada), the Commissariat à l’Energie Atomique and Institut National de Physique Nucléaire et de Physique des Particules (France), the Bundesministerium für Bildung und Forschung and Deutsche Forschungsgemeinschaft (Germany), the Istituto Nazionale di Fisica Nucleare (Italy), the Foundation for Fun-



(a) $m(p\pi^-)$ for $\bar{B}^0 \rightarrow D^+ p \bar{p} \pi^-$ with pdfs from the top: Breit-Wigner for X near $1.5 \text{ GeV}/c^2$ (top, blue); background pdf from (b) (bottom, red).

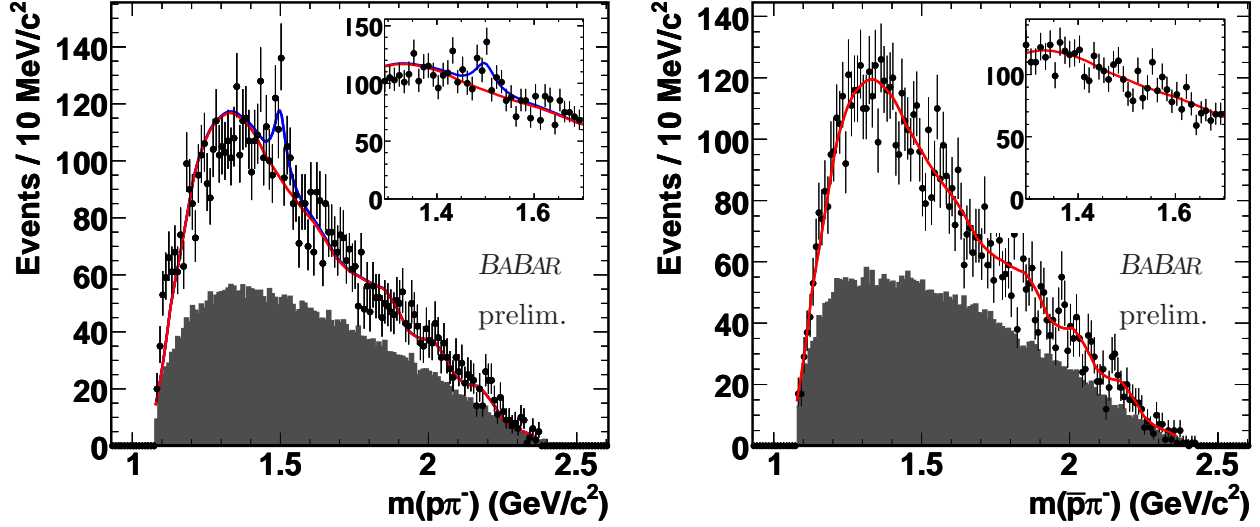
(b) $m(\bar{p}\pi^-)$ for $\bar{B}^0 \rightarrow D^+ p \bar{p} \pi^-$ with the smoothed histogram pdf used as background in (a).



(c) $m(p\pi^-)$ for $\bar{B}^0 \rightarrow D^{*+} p \bar{p} \pi^-$; see (a) for descriptions. (d) $m(\bar{p}\pi^-)$ for $\bar{B}^0 \rightarrow D^{*+} p \bar{p} \pi^-$; see (b) for descriptions.

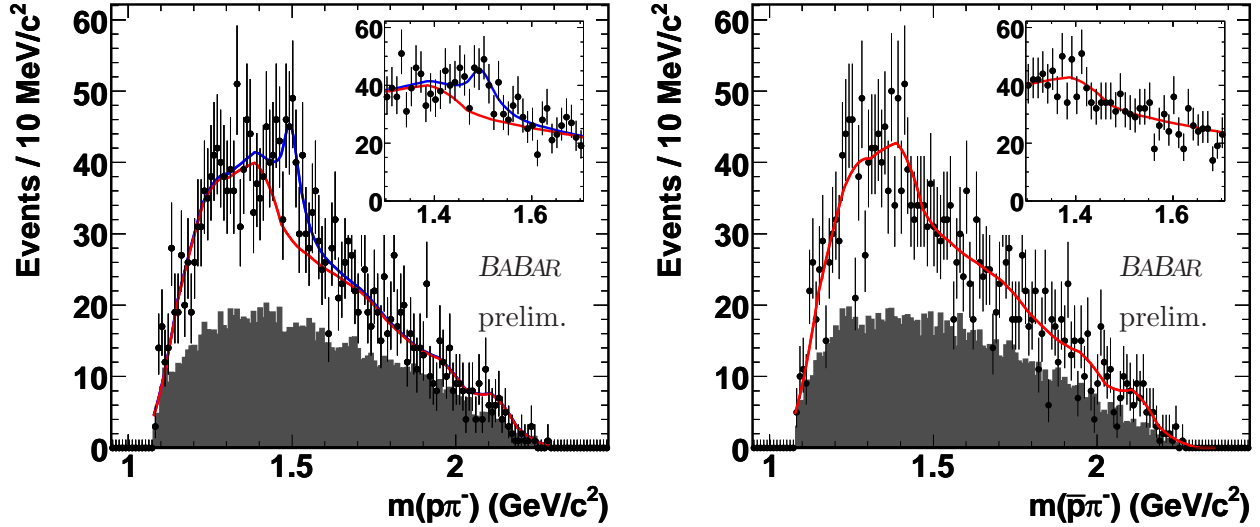
FIG. 11: Fits of $m(p\pi)$ in two neutral B decays: (ab) $\bar{B}^0 \rightarrow D^+ p \bar{p} \pi^-$ and (cd) $\bar{B}^0 \rightarrow D^{*+} p \bar{p} \pi^-$. The plotted sample are events in the signal box of $m_{\text{ES}} - \Delta E$ within 2.5σ of the mean; the grey histograms are the scaled sidebands. The in-set binning is the same as in the main figure.

damental Research on Matter (The Netherlands), the Research Council of Norway, the Ministry of Education and Science of the Russian Federation, Ministerio de Educación y Ciencia (Spain), and the Science and Technology Facilities Council (United Kingdom). Individuals have received



(a) $m(p\pi^-)$ for $B^- \rightarrow D^0 p\bar{p}\pi^-$ with pdfs from the top: Breit-Wigner for X near $1.5 \text{ GeV}/c^2$ (solid, blue); background from $m(\bar{p}\pi^-)$ in (b) (dashed, red).

(b) $m(\bar{p}\pi^-)$ for $B^- \rightarrow D^0 p\bar{p}\pi^-$ with the smoothed histogram pdf used as background in (a).

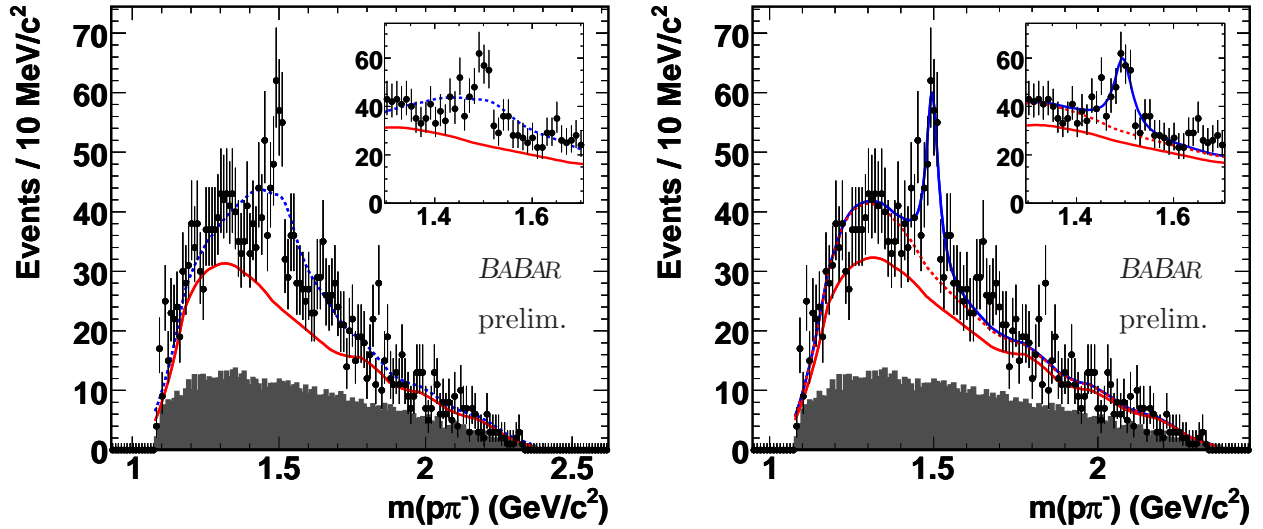


(c) $m(p\pi^-)$ for $B^- \rightarrow D^{*0} p\bar{p}\pi^-$; see (a) for descriptions. (d) $m(\bar{p}\pi^-)$ for $B^- \rightarrow D^{*0} p\bar{p}\pi^-$; see (b) for descriptions.

FIG. 12: Fits of $m(p\pi)$ in two charged B decays: (ab) $B^- \rightarrow D^0 p\bar{p}\pi^-$ and (cd) $B^- \rightarrow D^{*0} p\bar{p}\pi^-$. The plotted sample are events in the signal box of $m_{\text{ES}} - \Delta E$ within 2.5σ of the mean; the grey histograms are the scaled sidebands. The in-set binning is the same as in the main figure. Caveat empor: The fit for (a) has the width fixed to $51 \text{ MeV}/c^2$ found in Fig. 11a.

support from the Marie-Curie IEF program (European Union) and the A. P. Sloan Foundation.

-
- [1] J. H. Chen et al. [Belle Collaboration], Phys. Rev. Lett. **100**, 251801 (2008) [hep-ex/0802.0336].
 - [2] B. Aubert et al. [BABAR Collaboration], Phys. Rev. D **76**, 092004 (2007) [hep-ex/0707.1648].
 - [3] M. Z. Wang et al. [Belle Collaboration], Phys. Rev. D **76**, 052004 (2007) [hep-ex/0704.2672].
 - [4] T. Medvedeva et al. [Belle Collaboration], Phys. Rev. D **76**, 051102 (2007) [hep-ex/0704.2652].
 - [5] J. T. Wei et al. [Belle Collaboration], Phys. Lett. B **659**, 80 (2008) [hep-ex/0706.4167].
 - [6] B. Aubert et al. [BABAR Collaboration], Phys. Rev. D **72**, 051101 (2005) [hep-ex/0507012].
 - [7] Y. J. Lee et al. [Belle Collaboration], Phys. Rev. Lett. **93**, 211801 (2004) [hep-ex/0406068].
 - [8] X. Fu et al. [CLEO Collaboration], Phys. Rev. Lett. **79**, 3125 (1997).
 - [9] S. Anderson et al. [CLEO Collaboration], Phys. Rev. Lett. **86**, 2732 (2001) [hep-ex/0009011].
 - [10] I. Dunietz, Phys. Rev. D **58**, 094010 (1998) [hep-ph/9805287].
 - [11] K. Abe et al. [Belle Collaboration], Phys. Rev. Lett. **89**, 151802 (2002) [hep-ex/0205083].
 - [12] L. Wolfenstein, Phys. Rev. Lett. **51**, 1945 (1983).
 - [13] B. Aubert et al. [BABAR Collaboration], Phys. Rev. D **74**, 051101 (2006) [hep-ex/0607039].
 - [14] W. S. Hou, A. Soni, Phys. Rev. Lett. **86**, 4247 (2001) [hep-ph/0008079].
 - [15] C. K. Chua, W. S. Hou, S. Y. Tsai, Phys. Rev. D **65**, 034003 (2002) [hep-ph/0107110].
 - [16] C. K. Chua, W. S. Hou, S. Y. Tsai, Phys. Lett. B **544**, 139 (2002) [hep-ph/0204186].
 - [17] B. Kerbikov, A. Stavinsky, V. Fedotov, Phys. Rev. C **69**, 055205 (2004) [hep-ph/0402054].
 - [18] H. Y. Cheng, K. C. Yang, Phys. Rev. D **66**, 014020 (2002) [hep-ph/0112245].
 - [19] H. Y. Cheng, K. C. Yang, Phys. Rev. D **65**, 054028 (2002) [hep-ph/0110263].
 - [20] H. Y. Cheng, Nucl. Phys. Proc. Suppl. **163**, 68 (2007) [hep-ph/0607061].
 - [21] H. Y. Cheng, J. Korean Phys. Soc. **45**, S245 (2004) [hep-ph/0311035].
 - [22] H. Y. Cheng, K. C. Yang, Phys. Rev. D **67**, 034008 (2003) [hep-ph/0210275].



(a) $m(p\pi^-)$ fit with pdfs from top to bottom: known N^* (b) $m(p\pi^-)$ fit with pdfs from top to bottom: Breit-Wigner resonances at 1440, 1520, 1535, 1650 MeV/c^2 (dashed, for X (solid, blue); alternate background from $m(\bar{p}\pi^-)$ in blue); background from $m(\bar{p}\pi^-)$ in $D^+ p\bar{p}\pi^-$ (solid, red). $D^{*+} p\bar{p}\pi^-$ (dashed, red); background from $m(\bar{p}\pi^-)$ in $D^+ p\bar{p}\pi^-$ (solid, red).

FIG. 13: Alternate fits of $m(p\pi^-)$ in $\bar{B}^0 \rightarrow D^+ p\bar{p}\pi^-$. Known N^* resonances are used in (a) and an alternate background shape from $\bar{B}^0 \rightarrow D^{*+} p\bar{p}\pi^-$ is used in (b) as a systematic study. The in-set binning is the same as in the main figure. The grey histograms are the scaled $m_{\text{ES}}-\Delta E$ sidebands.

- [23] Z. Luo, J. L. Rosner, Phys. Rev. D **67**, 094017 (2003) [hep-ph/0302110].
 [24] M. Suzuki, J. Phys. G **31**, 755 (2005) [hep-ph/0501181].
 [25] J. L. Rosner, Phys. Rev. D **68**, 014004 (2003) [hep-ph/0303079].
 [26] J. L. Rosner, Phys. Rev. D **69**, 094014 (2004) [hep-ph/0312269].

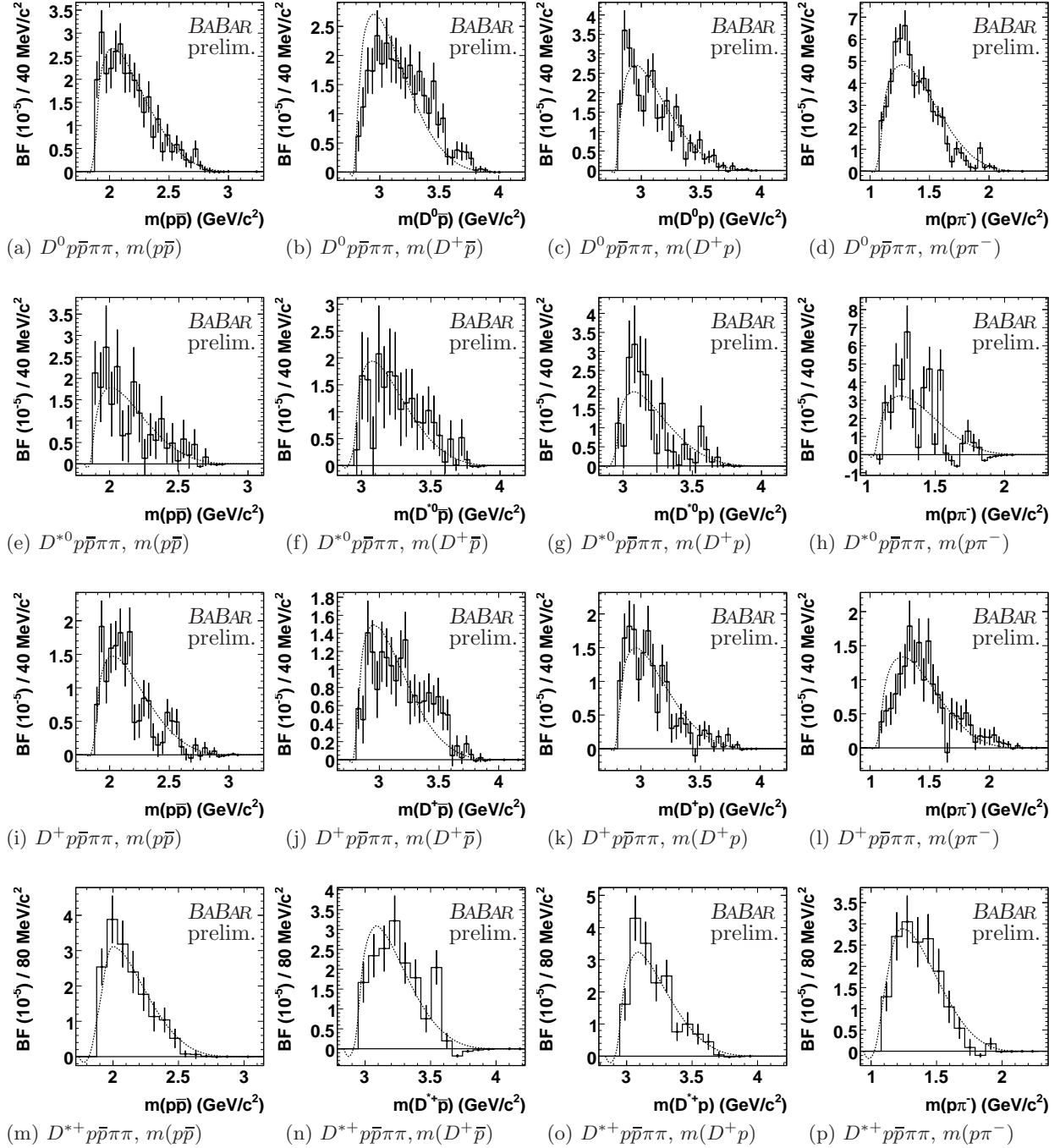


FIG. 14: 5-body B decay differential branching fractions as functions of $p\bar{p}$, $D^{(*)}p$, $D^{(*)}\bar{p}$, and $p\pi^-$ in (abcd) $\bar{B}^0 \rightarrow D^0 p\bar{p}\pi^-\pi^+$, (efgh) $\bar{B}^0 \rightarrow D^{*0} p\bar{p}\pi^-\pi^+$, (ijkl) $B^- \rightarrow D^+ p\bar{p}\pi^-\pi^-$, and (mnop) $B^- \rightarrow D^{*+} p\bar{p}\pi^-\pi^-$, respectively. The smooth curve represents decays following the uniform phase space model.

- [27] H. Y. Cheng, *Int. J. Mod. Phys. A* **21**, 4209 (2006) [hep-ph/0603003].
- [28] B. Aubert et al. [*BABAR* Collaboration], *Nucl. Instrum. Meth. A* **479**, 1 (2002) [hep-ex/0105044].
- [29] D. J. Lange, *Nucl. Instrum. Meth. A* **462**, 152 (2001).
- [30] T. Sjostrand, *Comput. Phys. Commun.* **82**, 74 (1994).
- [31] S. Agostinelli et al. [*GEANT4* Collaboration], *Nucl. Instrum. Meth. A* **506**, 250 (2003).
- [32] C. Amsler et al. [*Particle Data Group*], *Phys. Lett. B* **667**, 1 (2008). All nominal values used in the analysis are from this reference unless specified.
- [33] W. D. Hulsbergen, *Nucl. Instrum. Meth. A* **552**, 566 (2005) [physics/0503191].
- [34] B. Aubert et al. [*BABAR* Collaboration], *Phys. Rev. D* **65**, 032001 (2002) [hep-ex/0107025]. Sec. VII.C defines beam-energy-substituted B mass, B -beam energy difference, thrust, and the threshold pdf.
- [35] P. L. Frabetti et al. [*E687* Collaboration], *Phys. Lett. B* **331**, 217 (1994).
- [36] R. J. Barlow, *Nucl. Instrum. Meth. A* **297**, 496 (1990).
- [37] M. J. Oreglia, SLAC Report 236, App. D (1980); J. E. Gaiser, SLAC Report 255, App. F (1982).
- [38] F. James, M. Roos, *Comput. Phys. Commun.* **10**, 343 (1975).
- [39] W. Verkerke, D. Kirkby, *In the Proceedings of 2003 Conference for Computing in High-Energy and Nuclear Physics (CHEP 03), La Jolla, California, 24–28 Mar 2003, pp MOLT007* [physics/0306116].
- [40] R. Brun, F. Rademakers, *Nucl. Instrum. Meth. A* **389**, 81 (1997).
- [41] O. Long, *BABAR* Internal Note, BAD 54-7 (2001).
- [42] L. Lyons, D. Gibaut, P. Clifford, *Nucl. Instrum. Meth. A* **270**, 110 (1988).
- [43] M. Pivk, F. R. Le Diberder, *Nucl. Instrum. Meth. A* **555**, 356 (2005) [physics/0402083].
- [44] B. Aubert et al. [*BABAR* Collaboration], *Phys. Rev. Lett.* **98**, 012001 (2007) [hep-ex/0603052].
- [45] A. Aktas et al. [*H1* Collaboration], *Phys. Lett. B* **588**, 17 (2004) [hep-ex/0403017].
- [46] B. Aubert et al. [*BABAR* Collaboration], *Phys. Rev. D* **72**, 052006 (2005) [hep-ex/0507009].